BU
ARPA-E-45

Division of Engineering
BROWN UNIVERSITY
PROVIDENCE, R. I.

THE SEPARATION OF MEMBRANE AND BENDING SHEARS IN SHELLS WITH TWO BIREFRINGENT COATINGS

W. SCHUMANN, C. MYLONAS, and R. BUCCI

AD 657936

3 copies 1 - TL 1 - Mr. Zukas

1 - G. C. Klass

TECHNICAL LIBRARY
BLDG. 313
ABERDEEN PROVING GROUND, MD.
STEAP-TL

20060110136

National Science Foundation
Research Grant G 20259

Department of Defense
Advanced Research Projects Agency
Contract SD-86
Materials Research Program

NSF G20259
ARPA E45

June 1967

BU
ARPA-E-45

THE SEPARATION OF MEMBRANE AND BENDING SHEARS IN SHELLS WITH TWO BIREFRINGENT COATINGS[1]

by

W. Schumann[2], C. Mylonas[3], and R. Bucci[4]

Abstract

The directions and the differences of the principal membrane and bending stresses at a point of a shell or plate are calculated from the birefringence observed at normal incidence on two birefringent coatings, one on each face of the shell. A unique neutral surface is assumed, which is exact for identical coatings or for identical Poisson's ratios in shell and coating. Explicit formulas are obtained with the simplifying approximations of a negligible effect of the rotation of the principal directions and of a linear variation of the magnitude of the principal stress-difference over the finite coating thickness. These assumptions are strictly valid for very thin coatings, but give also reasonably good results for ordinary birefringent coatings.

TECHNICAL LIBRARY
BLDG 313
ABERDEEN PROVING GROUND MD.
STEAP-TL

---

[1] The results presented in this paper were obtained in the course of research sponsored in part by the National Science Foundation under Grant G-20259, by the Advanced Research Projects Agency under Contract SD-86, and by the Division of Engineering, and contains a modification of the report of reference (1) prepared under Contract DA-19-020-ORD-4674 of the Ballistic Research Laboratories of Aberdeen Proving Ground.

[2] Professor of Mechanics, Eidgenössische Technische Hochschule, Zurich, visitor at Brown University, 1956-57.

[3] Professor of Engineering, Brown University, Providence, Rhode Island.

[4] Research Assistant, Brown University, Providence, Rhode Island. This report is submitted as a thesis in fulfillment of a Master's Degree requirement at Brown University.

[redacted]

The validity of the derived expressions was checked experimentally in square plates subjected to anticlastic bending and membrane stress of known magnitude at various orientations. Two types of tests were performed. At first [1]* the membrane tension was applied through a series of pins in holes around the perimeter of a plate with relatively thick and optically insensitive coatings. Agreement between observed and calculated birefringence under these unfavorable conditions was reasonably good at the higher loads, but not good enough to permit an accurate inverse calculation of the stress-differences from the observed birefringence. The errors were found to be partly due to the difficulty of applying a true membrane force through pins without introducing any bending.

To assess accurately the new method, the troublesome pin loading method was abandoned and the membrane stress was simulated by a residual stress distribution in the coatings. The initial method of applying anticlastic bending was retained. Three plates were tested, a trial one with 0.164 in. thick coatings and two more with 0.108 ± 0.0015 and 0.057 ± 0.0015 in. thick coatings. At first the observed birefringence was compared with corresponding values calculated from the applied bending and membrane stresses. The real test of the proposed new method, however, was the inverse calculation of the principal bending and membrane stress differences from the birefringence observed on the two coatings. The agreement with the applied values was quite good, especially at the more interesting higher loads, even when a large rotation of principal stress occurred within one of the coatings.

List of Symbols

A, I	Effective cross-sectional area and moment of inertia per unit width of composite shell
C_σ	Stress optical coefficient in lb/(in x fringe)
E^*, E	Young's moduli of shell and coating, respectively
$M_1 \geqslant M_2$	Major and minor principal bending moments per unit width of shell, positive when causing tension at $z > 0$
$M = M_1 - M_2 \geqslant 0$	Principal difference of bending moments
$N_1 \geqslant N_2$	Major and minor principal membrane forces per unit width of shell
$N = N_1 - N_2 \geqslant 0$	Principal differences of membrane forces
$R = \Omega/\beta$	Ratio of the rate of rotation of the principal stresses in the wave front to half the rate of change of the relative phase difference at a point of the light path
$R_{av} = 2(\phi_{i1}-\phi_{i2})/n_i$	Ratio of the real rotation through the coating to half the retardation for single passage calculated from the real stress at mid-thickness.
S	$+ (1+R^2)^{1/2}$
$a_i > 0$	Distance from centroid of composite section to mid-thickness of coating above ($i = o$) or below ($i = u$)
$2H > 0$; $2h > 0$	Thickness of coated and uncoated shell, respectively
$h_i > 0$; $H_i > 0$	Distance from centroid of composite section to interface and to free surfaces of coatings respectively, above ($i = o$) or below ($i = u$), (Fig. 1)
$\Delta h_i > 0$	Thickness of coating above ($i = o$) or below ($i = u$)
$n_i \geqslant 0$	Fringe order ($\lambda = 5461$ Å) observed in reflected light on coating above ($i = o$) or below ($i = u$)
m	$(n_o^2 - n_u^2)/(n_o^2 + n_u^2)$
$n_{ti} \geqslant 0$; $n_{bi} \geqslant 0$	Fringe order observed above ($i = o$) or below ($i = u$) when shell is subjected only to membrane forces N_1, N_2, or only to bending moments M_1, M_2, respectively
n_z; n_{mi}; n_* all $\geqslant 0$	Fringe order which would appear under both M and N if the stress throughout the coating were equal to the total stress at a distance z; at the coating mid-thickness above ($i = o$) or below ($i = u$); or at a distance z_*
z	Distance from centroidal surface of composite shell, positive downwards

List of Symbols (continued)

α	Angle from the major principal membrane force N_1 to the major bending plane (M_1), ccw (counterclockwise) when viewed from below ($z > 0$)
2β	Rate of change of relative phase difference over a unit length due to birefringence with no rotation
γ_t, γ_b	Angle from the reference direction to the major principal membrane force N_1 and to the major bending plane (M_1), measured ccw positive when viewed from below ($z > 0$)
$\delta \geq 0$	$MAH/NI = (n_{bi}/n_{ti})H/a_i \geq 0$ (same for $i = o$ or $i = u$)
θ_{i2}, θ_z	Angles from the reference direction to the major principal total stress σ_1 at the surface of coating above ($i = o$) or below ($i = u$), or at distance z from the neutral surface, respectively. All angles measured ccw positive when viewed from below ($z > 0$)
ν^*, ν	Poisson's ratio of shell and coating, respectively
$\sigma^b_{1z} \geq \sigma^b_{2z}$	Major and minor principal bending stresses in the coating at distance z
$\sigma_{bz} = \sigma^b_{1z} - \sigma^b_{2z} \geq 0$, $\sigma_{bi} \geq 0$	Difference of principal bending stresses at a distance z and at mid-thickness $z = a_i$ of coatings above ($i = o$) or below ($i = u$). Their major principal directions are parallel to the corresponding major principal stress, hence change by 90° during passage from lower to upper coating
$\sigma^t_1 \geq \sigma^t_2$	Major and minor principal membrane stresses in the coating
$\sigma_t = \sigma^t_1 - \sigma^t_2 \geq 0$	Difference of principal membrane stress. Its major principal direction is parallel to σ^t_1
$\sigma_{1z} \geq \sigma_{2z}$	Major and minor total principal stress at distance z
$\sigma_z = \sigma_{1z} - \sigma_{2z} \geq 0$	Difference of principal bending stress at a distance z. Its major principal direction is parallel to σ_{1z}
ϕ_{i1}, ϕ_{i2}, or ϕ_z	Angle from the major total stress σ_1 to the major bending stress σ^b_1 at the plate-coating interface (1) and the free surface (2) of coating, above ($i = o$) and below ($i = u$), or at distance z, respectively. Angles are counterclockwise positive when viewed from below ($z > 0$)
Ω	Rate of rotation per unit length of the principal stresses in the wave front, positive when left-handed

Introduction

The determination of the surface strains of opaque bodies by the use of a cemented birefringent coating and reflected polarized light at normal incidence has been suggested by Mesnager [2] since 1930 and studied by Oppel [3] (1937). The method was first developed to practical use at Brown University [4-5] over thirteen years ago, and independently in France [6-7] and later in Japan [8]. This was made possible by the use of the highly strain-optically sensitive epoxy resins [5], which firmly adhere to many solids and may show several fringes even at a relatively small thickness and at strains as small as those of metal structures. The method allows the determination of the maximum in-plane shear strain at all points of the surface from a single picture almost as easily as in ordinary photoelasticity. This is exact for regions with small strain variations and far from the coating boundaries. In the presence of strong strain gradients and of curving of the surface, the strains vary through the thickness of the coating. Considerable errors [9] may result if the analysis is based on uniform strains over the thickness of the coating. In plates and smooth shells, strong variations of curvature or of strain in the metal-plastic interface over short distances (of a few coating thicknesses) are unlikely and the above errors should be negligible. However, another difficulty may arise from the superposition of bending and membrane stresses in the coating and their effect on polarized light. Pure bending produces a linear strain variation through the coating thickness which can be easily calculated from the resulting birefringence [14]. Pure membrane strains can also be directly determined from their optical effect since they are constant over the coating thickness. But the

superposition of bending and membrane loading at different principal directions produces principal stresses which vary in intensity and direction across the coating thickness. The photoelastic effect in such variable stress fields is very complicated [10-25] and no exact inverse solution for the stresses in terms of the total optical effect has been obtained.

Coatings of infinitesimal thickness, however, would obviously show no rotational effects, and very thin coatings would probably show very little. It appears interesting therefore to inquire whether in coatings of the usual thickness (0.050 to 0.250 in.) the total relative retardation may not also be, to an acceptable approximation, proportional to the integrated principal stress difference independently of rotation. The determination of bending and membrane stress from the total birefringence would then be relatively simple, and hopefully, sufficiently accurate. Obviously some modifications are needed for the determination of the <u>directions and differences of both principal membrane forces and of principal bending moments</u> at a point of a plate or shell. This is the only information which can be obtained from normal incidence measurements, which are independent of any in-plane isotropic state of stress. The individual principal components may be afterward determined with the help of additional observations at oblique incidence, or by some interferometric measurement of absolute retardations [33], or , for plates and thin shells, from the principal stress differences and directions by a method using integration from a boundary separatley for membrane and for bending stresses, as suggested by Akhmetzyanow [26].

Accordingly the main problem is to find the principal membrane and bending stress differences and directions. Four items of information are required to determine these four unknowns, and can be obtained from normal

incidence measurements with two birefringent coatings, i.e. from two relative retardations and two principal directions, as was shown earlier [1].

A similar problem, that of a shell with a reflective sheet at mid-thickness, has been recently treated by Kayser [23] and Kuske [24]. They consider the rotation of the stress and calculate the optical effect from the known stresses for a large number of cases. The inverse problem is then solved by comparison with the obtained direct solutions. The method would not be convenient for birefringent coatings as many direct solutions should be obtained for every ratio of metal to coating thickness. An approximate inverse solution for shells with thin birefringent coatings (coating about one tenth of plate thickness) has been recently made by Aben [25], on the basis of the differential equations of birefringence in inhomogeneous stress fields from observations with light of different wavelengths.

Analysis of the Stresses

Only the more likely method using coatings on both faces will be studied. The thickness of the metal shell or plate is $2h$, of the coated shell $2H$ and of the two coatings, above and below, Δh_o and Δh_u respectively (Fig. 1). The rectangular coordinate system has the axes x and y in the centroidal plane and the z-axis perpendicular to it and pointing downward ($z > 0$ below). The conditions of continuity of the tangential strains across the interface lead to the conclusion that normal in-plane forces per unit width $N_1 \gtrless N_2$ on two perpendicular planes give also rise to bending unless they are applied at specific distances from the mid-surface of the shell. In general these distances will be different in the two directions and will depend on the ratio $N_1 : N_2$, so that no effective centroid exists. Likewise bending moments per

unit width $M_1 \gtrless M_2$ in general result in bending about two different neutral axes in the two directions [28]. However for $N_1 \neq N_2$ and $M_1 \neq M_2$ a distinct neutral surface still exists when the two coatings are of identical thickness, or when shell and coating have equal Poisson's ratios. Then the principal membrane and bending stress-differences σ_t and σ_{bz} at a distance z in the coating, defined as positive quantities with principal direction parallel to the corresponding major stress, and the resulting positive birefringence n_i^t or n_i^b respectively, can be easily found from the corresponding positive principal differences N of membrane forces and M of bending moments (Fig. 1).

$$N = N_1 - N_2 \geq 0 \qquad M = M_1 - M_2 \geq 0 \tag{1}$$

$$\sigma_t = N/A \geq 0 \qquad \sigma_{bz} = |Mz/I| = \sigma_{bi}|z/a_i| \geq 0 \tag{2}$$

where σ_{bi} is the bending stress-difference at mid-thickness of coating i. Wherever possible formulas are given in terms of the fringe orders n_t and n_b which would be observed under pure membrane or bending loads, but can always be written in terms of N and M with the following substitutions

$$\left.\begin{aligned} n_{ti} &= 2\sigma_t \Delta h_i / C_\sigma = 2N\Delta h_i / AC_\sigma \geq 0 \\ n_{bi} &= 2\sigma_{bz} \Delta h_i / C_\sigma = 2Ma_i \Delta h_i / IC_\sigma \geq 0 \end{aligned}\right\} \tag{3a,b}$$

where the subscript i may be either o (denoting the coating above) or u (below), but the same in any one equation. The denominators A and I represent the effective area and moment of inertia per unit width of the coated shell, given in equations (4a, b) below in terms of the positive distances h_o and h_u from the neutral surface to the interfaces and a_o, a_u to

the mid-thickness of the coatings, the positive thicknesses Δh_o and Δh_u of the corresponding coatings (Fig. 1) and the Young's moduli and Poisson's ratios E^* , E and ν^* , ν of shell and coatings respectively. Expressions (4a, b) are exact when either $\Delta h_o = \Delta h_u$ or $\nu^* = \nu$, or when $N_1 = N_2$ and $M_1 = M_2$. The subscripts o (for over) and u (for under) indicate the side from the centroidal surface.

$$\left.\begin{aligned} A &= \frac{E^*(1-\nu)}{E(1-\nu^*)}(h_o + h_u) + \Delta h_o + \Delta h_u \\ I &= \frac{E^*(1-\nu)}{E(1-\nu^*)}[h_o^3 + h_u^3] + \Delta h_o[a_o^2 + \frac{1}{12}(\Delta h_o)^2] + \Delta h_u[a_u^2 + \frac{1}{12}(\Delta h_u)^2] \end{aligned}\right\} \quad (4a,b)$$

In general $\nu^* \neq \nu$, $\Delta h_o \neq \Delta h_o$, $N_1 \neq N_2$, $M_1 \neq M_2$ and no neutral surface exists. These values are then incorrect, but may be considered as good approximations because the differences between ν and ν^* , and between Δh_o and Δh_u are usually small.*

The total principal stress-differences and directions at a distance z after superposition of membrane and bending stresses can easily be found. The angles from a reference direction (Fig. 2) to the major membrane force N_1 , to the major plane of bending (M_1) and to the major total principal stress σ_1 at a distance z are γ_t, γ_b and θ_z respectively; the angle from N_1 to the major bending plane (M_1) is α and from σ_1 to the major principal bending stress σ_{bz} at z is ϕ_z ,

* When $\Delta h_o = \Delta h_u$ the neutral surface coincides with the middle surface: $h_o = h_u \cong h$. When $\Delta h_o \neq \Delta h_u$ but $\nu = \nu^*$ the position of the neutral surface is determined by:

$$h_o = \frac{4h^2E^*/E + 4h\Delta h_u - (\Delta h_o)^2 + (\Delta h_u)^2}{2(2hE^*/E + \Delta h_o + \Delta h_u)}$$

$$\alpha = \gamma_b - \gamma_t \tag{5}$$

$$\left.\begin{array}{ll} \phi_z = \gamma_b - \theta_z & \text{if} \quad z > 0 \\ \phi_z = \gamma_b - \theta_z + 90 & \text{if} \quad z < 0 \end{array}\right\} \tag{6}$$

and the positive quantity δ, identical for both sides, is defined as

$$\delta = MAH/NI = n_{bi}H/n_{ti}a_i \geq 0 \tag{7}$$

The stress difference $\sigma_z \geq 0$ at a distance z is easily written in terms of σ_t and σ_{bi}, or with the use of (2) and (7) in terms of σ_t, δ and z

$$\sigma_z^2 = \sigma_t^2 + 2\sigma_t\sigma_{bi}(z/a_i)\cos 2\alpha + (\sigma_{bi}z/a_i)^2 \tag{8}$$

$$\sigma_z^2 = \sigma_t^2[1 + (z\delta/H)^2 + 2(z\delta/H)\cos 2\alpha] \tag{8'}$$

with $z < 0$ and $i = 0$ for the coating above; and $z > 0$, $i = u$, below. The angle ϕ_z can be easily calculated, e.g. from Mohr's circle in Figure 4.

$$\cos 2\phi_z = (\cos 2\alpha + \delta z/H)\sigma_t/\sigma_z, \qquad \sin 2\phi_z = \sin 2\alpha \cdot \sigma_t/\sigma_z \tag{9}$$

At the free surfaces $z = \mp H_i$, ($-H_o$ above, $+H_u$ below) and $\phi_z = \phi_{i2}$, (ϕ_{o2} or ϕ_{u2}), hence

$$\left.\begin{array}{l} \sin 2\phi_{i2} = \sin 2\alpha \Big/ \sqrt{1 \mp 2(\delta H_i/H)\cos 2\alpha + (\delta H_i/H)^2} \\ \cos 2\phi_{i2} = (\cos 2\alpha \mp \delta H_i/H) \Big/ \sqrt{1 \mp 2(\delta H_i/H)\cos 2\alpha + (\delta H_i/H)^2} \end{array}\right\} \tag{9'}$$

where the upper sign should be taken with $i = o$ (coating above) and the lower sign with $i = u$ (coating below). In addition, from (6)

$$\theta_{u2} - \theta_{o2} = \phi_{o2} - \phi_{u2} + 90 \tag{10}$$

The proper quadrant for $2\phi_{u2}$ is found from the signs of their sine and cosine in the usual way. For $2\phi_{o2}$ the regular angle must be changed by ±180° (Fig. 5).

It should be noted that for $z > 0$ the positive bending stress difference σ_{bz} makes with σ_t the same angle α as the major bending plane makes with N, but for $z < 0$ the angle is $\alpha + 90$ according to the definition of the stress-difference as positive and parallel to the major principal stress. However the same angle 2α appears in all expressions for both coatings, but the proper sign is determined by the value of z, except in expression (8') where the coating dimensions H_i are taken with the proper sign, positive for the coating below $(i = u\ ,\ H_u > 0)$ and negative above $(i = o\ ,\ H_o < 0)$.

Alternatively the direction of the bending stress-difference could be identified with the plane of major bending and its magnitude would be positive for $z > 0$ (when the major stress is parallel to the plane of bending) and negative for $z < 0$ (when the minor stress is parallel to the plane of bending). The final formulas, however, must be expressed in terms of observed relative retardation or fringe order, which is proportional to the stress-difference, hence would also be positive or negative. This scheme would be acceptable for uniaxial stress, as e.g. for a beam under tension and bending as in Fig. 1, as well as in ordinary plane-stress photoelasticity whenever no doubt exists as to the sign and direction of the stress, (e.g. at the free boundary which is the region of main interest). In general, however, the tensorial variation cannot be escaped and

complications arise. If the stress difference causing one fringe is defined as positive when the major principal stress has a fixed direction and negative when it is perpendicular to it, then the same circular fringe, e.g. in the problem of a shrink fit (Fig. 12a) would be fringe +1 at two diametral points and fringe -1 at the diametral points of the perpendicular diameter. All other points would have undetermined sign, as the major principal stress has none of the previous two directions. Obviously the first definition is preferable and was adopted. The only inconvenience is the apparently discontinuous jump by 90° of the direction of the stress-difference, whereas under the alternative definition, it would have only changed sign. In most formulas, however, the same change of sign could be attributed either to an always positive σ_z or n_z and a changing $\cos 2\alpha$ to $\cos 2(\alpha + 90)$ or to a fixed $\cos 2\alpha$ and a sign change in σ_z .

Birefringence in Inhomogeneous Stress Fields

The first study of birefringence in inhomogeneous stress fields appears to be the work of Neumann [10] who gave the differential equations governing the intensity and phase retardation of the components polarized along the principal stresses for any variation of azimuth and intensity of stress-difference along the light path. Poincare [11] in a general study of light gave the most elegant representation of birefringence on a unit sphere. More recently Drucker and Mindlin [12] solved the problem of wave propagation in a stressed medium of constant rate of rotation Ω of the principal directions per unit distance along the ray (i.e. as a screw of constant pitch) and constant stress-difference, which in the absence of rotation would have caused a rate of change 2β of phase difference per unit distance. After neglecting

some terms, which are extremely small for all practical photoelastic materials and rates of rotation, they reached explicit expressions for the amplitude and the phase difference of the components of vibration along the local principal stress axes at each point in terms of the dimensionless ratios $R = \Omega/\beta$ and $S = +(1 + R^2)^{1/2}$. Each component of vibration parallel to a principal stress at incidence gives rise at a distance x to two components, one parallel to the local (rotated) principal stress and another transverse and $(R/S)\sin(S\beta x)$ time smaller. The transverse component vanishes only at retardations of integer wavelengths $(2\beta SX = 2k\pi)$. Accordingly the incident polarization re-appears at integer wavelengths at the same angle to the local stress axes as at incidence and extinction may be achieved with the analyzer likewise rotated, but the fringes will correspond to a birefringence S times larger than if the stresses did not rotate. This may be shown [27] to hold also for R variable and for reflection at integer plus one-half wavelength retardations and return through the same path, as in birefringent coatings. At intermediate retardations the second component, if at all significant, will produce an ellipse of polarization bearing little resemblance with the ordinary ellipse in the absence of rotation and will render the isoclinics indistinct and erroneous. The second passage of the light back through the coating does not cancel the rotational effects and increases the complication.

Drucker's and Mindlin's results are a special solution of Neumann's equations for a constant R, and though correct, show an unnecessarily large rotational effect because they give the new components of polarization along the rotated stress axes. A part of the correction is just a transcription of the ellipse of polarization in the new axes and the

remainder is the pure rotational effect. Drucker's and Mindlin's correction increases continuously with R and S whereas the error in the polarization ellipse in fixed coordinates can be shown to be highest for $R = 1$ and to diminish to zero for R tending to zero or to infinity [27]. This may also explain why rotational effects were not noticeable in a thin twisted tape subjected to light axial pull and having a very high rotation at a small retardation [29], but became quite pronounced under a stronger axial pull causing a reduction in R [27].

The first application of the effect of stress rotation was made by Drucker [15] in a photoelastic study of plates subjected to bending at an angle to an initial frozen-in tension, permitting the detection of the otherwise self-anulling birefringence due to bending. The direction and magnitude was known and only the direction and difference in principal bending moments, hence two unknowns, were sought from a single photoelastic observation. That problem was simpler than the one of the present paper in which 4 unknowns (2 directions, 2 stress-differences) are sought from 2 photoelastic observations.

A general study of birefringence in inhomogeneous stress fields in media with linear constitutive relations was done by Mindlin and Goodman [16]. They have shown that even in the absence of rotation the ordinary photoelastic law is an approximation if the stress field contains gradients along the ray, as also shown by Mindlin [14], or across it. With additional approximations, similar to those of Drucker and Mindlin [12], they reached general differential equations which for harmonic waves reduced to Neumann's equations. No explicit solution has been obtained, except for R constant, but it was shown that the solution would mainly

depend on the variation of R along the light path. The most systematic study has been made by Aben [19,20] with matrix operators.

It is not always realized that birefringence with optical activity (rotating power) in crystals is identical with birefringence in rotating stress fields. In the stress-fields the electric vector tends to remain parallel and the principal directions rotate, whereas in the active crystal the electric vector is rotated and the principal birefringence directions remain unchanged. Accordingly many results obtained in physical optics (such as the rotation of certain orthogonal elliptical vibrations without change of ellipticity) may be directly applied to uniformly rotating stress fields. Likewise the methods of the Poincaré sphere [11,17] and of matrix operators [13,17-20] offer excellent means for the visualization and calculation of stress birefringence effects. Some of these results have frequently been re-derived as variants for special applications. An interesting method consisting essentially of a plane projection of the Poincaré sphere was derived by Menges [21] and Kuske [22]. Wood [30] studied the vibration modes of crystal plates with rotating power. Mark [31] has calculated the combination of bending and tension of plates giving clear isoclinics. Stress determination in rotating stress fields by scattered light was suggested by Menges [21] and separately with a special technique by Robert and Guillemet [34,35].

The stress distribution in the present problem is only slightly more general than in the problem of the twisted tape [29]: it is a superposition of a uniform tension on a linearly variable bending stress at an angle α which may vary from 0 to 180°, instead of being always at 45°. On the other hand the bending stress variation is much smaller across the coating than over the whole coated shell, hence the rotation is frequently

small, negligibly so with very thin coatings. Certainly no rotational effect should be expected at points of the plate where the principal directions of bending and tension form angles of 0 or 90° because the linear distribution of stresses along the light path do not give rise to measurable discrepancies from the simple photoelastic law [14, 16]. Furthermore, when either stress is much stronger than the other, the rotation is very small and without effect on the relative retardation. Some indication of the probable rotational effect on the birefringence may be obtained from the average value of R across the coating thickness (calculated as the ratio of the rotation to half the retardation for single passage through the coating with uniform stress equal to the stress at mid-thickness). Figures 3a, 3b show graphs of R_{avg} vs. the angle α for membrane and bending fringe orders n_t and n_b respectively in 0.108 in. (Fig. 3a) or 0.057 in. thick coatings (Fig. 3b) on a 0.250 in. thick shell. Obviously significant rotational effects should be expected when n_t and n_b are small and about equal and simultaneously the angle α is between about 70° and 110° but not very close to 90°, as then no appreciable error is expected (all the rotation then occurs in the region where the stress is negligible, hence R is very large and the effect small).

The rotation and change of magnitude of the total principal stress through the coating thickness can be easily visualized on a Mohr diagram. As the photoelastic effect depends on principal stress differences, it is permissible to consider both membrane and bending stresses as equivalent states of pure shear, $\sigma_1^t = -\sigma_2^t = \frac{1}{2}\sigma_t$ and $\sigma_{1z}^b = -\sigma_{2z}^b = \frac{1}{2}\sigma_{bz}$. For anticlastic bending this is exact; for other problems the true state will differ by an isotropic stress, which anyway cannot be determined from

simple photoelastic observations at normal incidence at a point. These assumptions may shift the origin of Mohr's circle but do not affect its diameter and they greatly simplify the superposition of the stress-differences. Figure 4 (top) shows the separate membrane and bending stress states and their superposition at a general point in the coating below ($z > 0$) and in a symmetric point ($z' < 0$) in the coating above as seen from some point $z >> 0$. The membrane stress σ_t is identical at the two points, but the bending stress-difference σ_{bz} , positive by definition, is at an angle α to σ_t for $z > 0$ and at $\alpha + 90$ for $z' < 0$. The superposition is carried out in Mohr's diagram by drawing first the circle for $\sigma_t > 0$ (Fig. 4), determining the points A and B on the circumference at angles 2α and $2(\alpha + 90°)$ and adding the suitable bending stresses $\frac{1}{2}\sigma_{bz}$ and $-\frac{1}{2}\sigma_{bz}$ to find the points A_u, B_u (coating below) or A_o, B_o (coating above), which represent the total secondary stresses in the principal bending directions. Mohr's circle drawn on A_uB_u (or A_oB_o) as diameter represents the total state of stress at z (or z') and these diameters represent the corresponding total stress-difference. The angle ϕ_z from the major principal total stress σ_{1z} to the major bending stress is also shown.

The variations of stress through the coating thickness can be found on a similar diagram simply by varying the magnitude of the bending stress $\frac{1}{2}\sigma_{bz}$, i.e. the lengths of AA_u and BB_u , etc. For example, Figure 5 shows the superposition of membrane and bending stress differences at the free surface (diameter $A_{u2}B_{u2}$) and at the metal-coating interface (diameter $A_{u1}B_{u1}$) of the coating below, and similarly for the coating above (diameters $A_{o2}B_{o2}$ and $A_{o1}B_{o1}$ respectively). The corresponding Mohr's

circles need not be drawn. The angles ϕ_{u2} and ϕ_{u1} of the major total stress at the free surface and at the interface of the coating below with the major bending stress are easily found, and also the corresponding angles ϕ_{o2} and ϕ_{o1} in the coating above. The total rotation $\phi_{u2} - \phi_{u1}$ across the thickness of the coating above is much larger than the rotation $\phi_{o2} - \phi_{o1}$ below. The orientation α of σ_b in relation with σ_t, i.e. the position of point A, greatly influences the total rotation through the coating, even for constant σ_t and σ_b.

The points P'_u, P''_u represent the stress state at a distance $z > 0$. Their position along the segments $A_{u1}A_{u2}$ and $B_{u1}B_{u2}$ varies proportionally with the bending stress-difference, hence proportionally with z. Twice the length OP'_u gives the corresponding total principal stress-difference σ_z and half the angle DOP'_u gives the angle of σ_z to the constant direction of σ_{bz}. Obviously point C_u gives the lowest stress-difference and the highest rate of rotation per unit change of z, hence gives the highest ratio R. When this point lies in the coating and the distance from 0 to AA_{u2} is small, the total rotation through the coating should be large and the stress small, hence the effects on polarization could be significant. In the coating below this situation arises when α approaches 90° (point A close to C) and simultaneously the bending stress at the coating mid-thickness is about equal to σ_t. For the coating above α should approach zero. This was also the conclusion reached from the graphs of R_{avg} vs. α (Fig. 3a, b), but it must be remembered that angles equal to or very close to 90° or 0° will cause no rotational errors.

It is clear that the region of highest rotation may lie outside both coatings and then the effects of rotation on fringe order and on isoclinics may be very small. Even when this region lies within a coating, the effect may not be severe, as e.g. in the early tests with a twisted tape. These conclusions spurred the hope that a practical and sufficiently accurate method for finding the stresses in shells might be developed even though the exact effects of rotation are not taken under consideration. The proposed method is important and useful not so much for finding the birefringence once the stresses are known, which can be easily found by integrating Neumann's equations by steps (or using Poincaré's sphere or matrix operators), but for the inverse problem of finding the stresses from the birefringence on the two coatings. The integrated effects of birefringence and rotation in the two coatings cannot be solved for the stresses, whereas the proposed simplified algebraic expressions can. The accuracy of the proposed method has generally been found good, though somewhat less so with a few combinations of M , N, α causing a high rotation in one coating.

Calculation of the Birefringence

The fringe order, if independent of rotation, would be found as the integrated photoelastic effect during the forward and backward passage through each coating of thickness h_i

$$n_i = \frac{2}{C_\sigma} \int_{h_i}^{H_i} \sigma_z dz \tag{11}$$

with $i = o$ for the coating above and $i = u$ below. Substitution of σ_z as in (8'), integration and substitution of fringe orders for stresses from (3), gives

$$n_i = n_{ti}(H/2\delta\Delta h_i)\left|A_i - B_i + \sin^2 2\alpha \ln(A_i/B_i)\right| \tag{11a,b}$$

and in terms of an always positive H_i (i.e. $H_u > 0$, $H_o > 0$)

$$A_i = (\delta H_i/H \mp \cos 2\alpha)\sqrt{(\delta H_i/H \mp \cos 2\alpha) + \sin^2 2\alpha}$$

$$B_i = (\delta h_i/H \mp \cos 2\alpha)\sqrt{(\delta h_i/H \mp \cos 2\alpha) + \sin^2 2\alpha}$$

Equation (11a) for $i = o$ and the upper of the double signs gives the integrated fringe order n_o for the coating above; Eq. (11b) with $i = u$ and the lower signs gives the fringe order below. The factor $(n_{ti}H/\delta\Delta h_i)$ is the same for both coatings and equal to $NH/A\delta C_\sigma$ which may be substituted if n_i must be expressed in terms of N instead of n_t . For identical coatings $h_i/H = h/H$, $H_i/H = 1$ and $n_{ti} = n_t$, but $n_o \neq n_u$. These equations are more complicated than the one given by Drucker [15], as they contain the three basic parameters n_t (or N), δ , and α as well as the ratio h/H .

<u>Inverse Solution for Membrane and Bending Stress-Differences</u>

In the inverse solution it is required to determine n_b, n_t, α and γ_b , or the equivalent δ , n_t, α, γ_b , from the experimental measures of n_o, n_u, θ_{o2} and θ_{u2} . However, once δ and α are found γ_b is easily determined from (9') and (6). Essentially the problem then consists of finding the three quantities δ, n_t and α in terms of n_o, n_u and

$\theta_{u2} - \theta_{o2}$ and requires three independent equations in these variables. If equations (11a,b) are used the solution will have to be numerical. A very simple explicit solution can be obtained with a further approximation which is justified by the test results. For thin coatings the principal stress difference is assumed linear across the coating thickness. With this assumption the observed fringe order n_i may be taken equal to the fringe order of a coating with a uniform stress equal to the real stress at mid-thickness $z = a_i$. Two equations are obtained from expression (7) for $z = a_i$ after multiplication throughout by $2\Delta h/C_\sigma$ to transform stresses into fringe orders:

$$n_i^2 \cong n_{mi}^2 = n_{ti}^2 \mp 2n_{ti}n_{bi} \cos 2\alpha + n_{bi}^2 \tag{12}$$

with $i = o$ and the upper sign for the coating above, or $i = u$ and the lower sign for the coating below.

For identical coatings, $n_{ti} = n_t$, $n_{bi} = n_b$ and $a_i = a$, but $n_o \neq n_u$. Addition and subtraction and substitution of (7) gives

$$\left.\begin{aligned} n_u^2 + n_o^2 &= 2n_t^2(1 + \delta^2 a^2/H^2) \\ n_u^2 - n_o^2 &= 4n_t^2(\delta a/H)\cos 2\alpha \end{aligned}\right\} \tag{13}$$

Division of the first by the second Eq. (13) gives

$$\cos 2\alpha = m \,\frac{1+\delta^2 a^2/H^2}{2\delta a/H} \tag{14}$$

where

$$m = (n_u^2 - n_o^2)/(n_o^2 + n_u^2) \tag{15}$$

The third independent equation is obtained from the calculation of $\cos 2(\theta_{u2} - \theta_{o2})$ after the substitution (10), expansion and substitution of (9') for $H_i = H$, or directly from a Mohr diagram as in Fig. 4.

$$\cos(\theta_{u2} - \theta_{o2}) = -\cos(\phi_{o2} - \phi_{u2}) = (1 - \delta^2) \Big/ \sqrt{(1 + \delta^2)^2 - 4\delta^2\cos^2 2\alpha} \qquad (16)$$

Substitution of $\cos 2\alpha$ from (14) and solution for δ^2 gives:

$$\delta^2 = \frac{[1 - \quad 1-m^2 \cos 2(\theta_{u2} - \theta_{o2})]^2 - A}{1 - (1-m^2a^2/H^2)\cos^2 2(\theta_{u2} - \theta_{o2})} \qquad (17)$$

where A is the quantity

$$A = 2\cos 2(\theta_{u2} - \theta_{o2})\left\{\sqrt{1-m^2} - \sqrt{1-m^2-m^2\sin^2 2(\theta_{u2} - \theta_{o2})\Delta h^2/4aH}\right\} \qquad (18)$$

The value of <u>A is zero</u> for the following cases:

I. $m = 0$, i.e. $n_o = n_u$, which occurs when

a) $n_b = 0$ and therefore $n_o = n_u = n_t$ and $\theta_{u2} - \theta_{o2} = 0$

b) $n_t = 0$ and therefore $n_o = n_u = n_b$ $2(\theta_{u2} - \theta_{o2}) = \pm 180°$

c) $n_t = n_b H/a$, and it can then be shown that $2(\theta_{u2} - \theta_{o2}) = \pm 90°$ for any value of α.

II. $m = 1$, i.e. $n_o = 0$, which occurs when $n_t = n_b$ and $\alpha = 0$. Then the angles θ_{o2} and therefore $2(\theta_{u2} - \theta_{o2})$ cannot be experimentally determined, but for $\alpha = 0$ Eq. (16) shows that $\sin 2(\theta_{u2} - \theta_{o2}) = 0$.

III. $m = -1$, i.e. $n_u = 0$, which occurs when $n_t = n_b$ and $\alpha = 90°$. Again Eq. (16) shows that $\sin 2(\theta_{u2} - \theta_{o2}) = 0$.

The value of A is also zero for intermediate values of m , $-1 < m < 0$ and $0 < m < 1$, when the coating is infinitesimal. For thin coatings $(\Delta h << H)$ A is small and has been neglected in all present calculations.

The value of A may serve as a check of the experimental data. With the correct values of m and $\theta_{u2} - \theta_{o2}$ the quantity under the second square root in A should be positive, since a real δ always exists (including $\delta \to \infty$ for $n_t = 0$).

$$1 - m^2 - m^2\sin^2 2(\theta_{o2} - \theta_{u2})\Delta h^2/4aH \geq 0 \tag{19}$$

Experimental data not fulfilling (19) would indicate measurement errors or appreciable rotational effects. One could then accept a further approximation, either by "conditioning" the data to fulfill (19), or by neglecting the quantity A . In the present tests A was neglected, but only after checking for the fulfillment of (19) by each set of measurements. Violation of (19) could possibly occur at angles α close 90° for the coating below, or 0° above and for $n_b < n_t < n_b H/a$, when m approaches 1 but is not so close as to make A almost zero (as in II and III above). These are also the conditions giving the strongest rotation so that errors would not be unexpected.

After δ is found from (17), the value of n_t is found from the first of (13) and of n_b from (7)

$$n_t^2 = \frac{1}{2}(n_u^2 + n_o^2)/(1 + \delta^2 a^2/H^2) \tag{13}$$

$$n_b = n_t \delta H/a \tag{7}$$

Finally the value of α is found from (14). Calling $2\bar{\alpha}$ the 1st quadrant solution of (14) when $\cos 2\alpha > 0$ or $m > 0$ or the 2nd quadrant solution when $\cos 2\alpha < 0$ or $m < 0$, the solution for 2α is

$$2\alpha = 2\bar{\alpha} \quad \text{when} \quad 0 < 2(\theta_{u2} - \theta_{o2}) < \pi \quad \text{or} \quad -\pi < 2(\phi_{o2} - \phi_{u2}) < 0$$

$$2\alpha = -2\bar{\alpha} \quad \text{when} \quad -\pi < 2(\theta_{u2} - \theta_{o2}) < 0 \quad \text{or} \quad 0 < 2(\phi_{o2} - \phi_{u2}) < \pi$$

The computed values of n_t, n_b and α give the magnitude of the membrane and bending "stress-difference" and their relative angle. Their absolute directions γ_t, γ_b can easily be found from (9'), (6) and (5), as already mentioned. Instead of either of (9') it is easier to use their quotient to find ϕ_{u2}:

$$\tan 2\phi_{u2} = \sin 2\alpha / (\cos 2\alpha + \delta) \tag{20}$$

with the usual quadrant selection according to the signs of numerator and denominator.

Test Methods

The tests had two purposes: to check the accuracy of the direct formulas (8') and (11) or (12) giving the total birefringence in terms of the applied membrane and bending stresses and, if these proved accurate enough, to check the inverse formulas (15)-(17) and (10') giving the applied membrane and bending stresses (or corresponding birefringence and their relative direction) in terms of the observed fringe orders and principal directions on the two coatings. Two types of tests were made, both with doubly coated square plates subjected to anticlastic bending and to in-plane tension of variable direction.

In both series of tests anticlastic bending was produced by transverse forces Q applied at a pair of diagonally opposed corners and $-Q$ at the other pair, which caused principal bending moments $M_1 = -M_2 = \frac{1}{2} Q$ or $M = Q$, with principal directions parallel to the plate diagonals.

<u>First Series of Tests</u>. In the first series in-plane tension was produced by forces P evenly distributed through a system of beams and levers at 16 points of the half-perimeter of the plate, 8 on each side, at an angle α to the diagonals which could be varied between 45° and -45° (Figs. 6, 7).

Anticlastic bending deformed the plate into a hyperbolic paraboloid. To cause only membrane stress the 16 loads on the perimeter should be tangential to the deformed plate. This could be approximated by an out-of-plane tilt of the system of levers about the midpoints H (Fig. 6), adjusted after several trials to the point where a change of P from zero to its highest value would cause no variation of the already applied Q. The adjustment was generally difficult, lengthy and imperfect, except when α was equal to 0° or 45°. As a consequence an unknown small stress system was introduced and caused errors. Other sources of error were the imperfect centering of the pins about the mid-plane of the plate and of the levers, and the unavoidable location of the pins in holes lying a short distance inside the edges of the plate. Halfway between the holes the edge was slotted to the depth of the centerline of the holes, which thus determined the size of the square subjected to tension. On the other hand, to achieve an exact anticlastic loading over the whole plate, the loads Q had to be applied precisely at the corners of the original square, which was larger than the one subjected to tension. A compromise was reached by slotting

only the plate and not the birefringent coatings so that at the slots the plate was weak in tension but could take a good part of the bending. Therefore, to a first approximation, the tension was applied to an 8" square and the bending to a 9" square.

The plate was 0.248 in. thick 24ST aluminum, and the coatings were selected relatively stress-free $\frac{1}{4}$" thick sheets of CR39. The small sensitivity and considerable thickness permitted an assessment of the present method under unfavorable conditions.

The values of the various quantities were:

$2h = 0.250$ in	$H_o = 0.3705$ in	$E = 2.86 \times 10^5$ psi
$\Delta h_o = 0.245$ in	$H_u = 0.3955$ in	$\nu = 0.40$
$\Delta h_u = 0.271$ in	$a_o = 0.248$ in	$A = 9.90$ in^2/in
$h_o = 0.1255$ in	$a_u = 0.260$ in	$I = 0.853$ in^4/in
$h_u = 0.1245$ in	$E^* = 1.02 \times 10^7$ psi	$C_\sigma^+ = 78$ lb/in(in. fringe)
$2H = 0.766$ in	$\nu^* = 0.33$	

The inequality of the two coatings had a very small influence on the position of the centroid (0.001" off mid-thickness) and an altogether negligible effect on the effective moment of inertia. All calculations were made with the expressions for assymetric coatings.

These first tests served to verify expressions (11) or (13') for total birefringence and (8') for its principal direction. Observations were made only on the coating below. Plane polarized light was used at the azimuth giving the brightest fringe pattern. Rather than apply arbitrary values of

+ Determined by a test in pure anticlastic bending.

N and M (or n_{tu} and n_{bu}) and 2α and then check the observed vs. the calculated values of n_u and θ_{u2} , M was applied first and then N was increased, at a constant direction, till the first fringe order was observed. For $i = u$, the lower sign (+) and $n_u = 1$, Equation (12) represents a family of central ellipses with semi-axes along the bisectors of the coordinate axes n_b, n_t equal to $0.707\sec\alpha$ and $0.707\operatorname{cosec}\alpha$, and passing through the points ($n_b = \pm 1$, $n_t = 0$) and ($n_b = 0$, $n_t = \pm 1$). Figure 8 shows these ellipses and the corresponding experimental points (i.e. the values n_t, n_b which in the test caused one fringe at angles α equal to 0°, 15°, 30°, 45° and 90°).

As the principal directions could not be easily detected when the whole plate was covered with the dark first fringe, the loads were reduced by $\frac{1}{2}$ and the crossed polaroids were rotated to give minimum light intensity. In irrotational photoelasticity this would have given the true isoclinic at $\frac{1}{2}$ as well as 1 fringe.

At angles α equal to 60° and 75° the tension needed to produce one fringe exceeded the capacity of the machine even when the bending was light. Tests were then made with polarizer and analyzer parallel (light field) and membrane and bending intensities adjusted to give a black fringe, which in ordinary irrotational photoelasticity would correspond to a fringe order of $\frac{1}{2}$. Of course the rotational effect at a retardation of $\frac{1}{2}$ wavelength is stronger than at one wavelength, and must have influenced the fringe order as well as the direction. In addition the 90° rotation of the analyzer introduced further complications, but it was still desirable to test the suitability of this approximate method under such conditions.

Agreement between analytical and experimental fringe orders was excellent at $\alpha = 0°$ and reasonably good at $\alpha = 15°$, $30°$ and in part at $45°$, with loads producing a retardation of one fringe ($n = 1$), but not so good at $\alpha = 60°$ and $75°$ and with the lower loads producing only half a fringe ($n = \frac{1}{2}$). A significant part of the errors was caused by pin-loading in tension, as already discussed and indicated by the uncertainty in the load needed to cause one fringe even in simple tension (Fig. 8, points on vertical axis), when the plate had no curvature. The errors were increased by the bending curvature, by appreciable initial stresses and by viscoelastic effects, especially after prior loadings. The principal directions, however, showed such a high discrepancy that no attempt was made to solve inversely for the applied membrane and bending stresses in terms of the observed birefringence on the two coatings.

Second Series of Tests

a. The Plate. The purpose of the second series of tests was to increase the accuracy and check the inverse solution for membrane and bending loads in terms of observed birefringence on the two faces. The tests were therefore designed so as to remove the uncertainty of pin-loading and to reduce the errors due to the excessive thickness, to the low sensitivity and to the viscoelastic behavior of the previously used coatings. To avoid pin-loading or clamping and the resulting transverse constraint, it was decided to simulate the membrane stress by a uniform residual tension imposed on the coatings before cementing them to the plate. Anticlastic bending would be applied as before. The difficulty of uniformly stressing a 9 x 9 in. plate, however, would not be overcome but only transferred from the plate to

the coating. Furthermore pairs of identical coatings would have to be stressed to various intensities and be cemented with their principal direction at various angles to the diagonals. It was then recognized that the strived-at uniformity of stress over the whole plate was not essential, since each test required an observation at only one point on each coating. Pairs of coatings with identical residual stress fields, but variable so as to include all required magnitudes and directions, would permit the use of a single carefully coated plate for all tests. Each test would again consist of observations at two corresponding points, one on each coating, having the desired magnitude and direction of membrane stress. Although in the present tests the residual stress fields of the two faces were identical to a high degree of accuracy, this requirement could have been relaxed, since anticlastic bending was uniform over a large central area of the plate. With the dimensions and loads used the errors from edge effect, membrane action and transverse shear [32] should be less than 0.002 in. a central 5 in. diameter circle. Observations could then be made at any two points, one on each face, having identical membrane stress, even if they would not lie on the same normal to the mid-plane.

Several methods were tried for casting the araldite sheets used as coatings. Most methods caused residual stresses, cracking, or an uneven thickness. The final and most successful method, perfected after many trials, used specially machined 13 x 15 x 3 in. aluminum molding plates ground flat within ±0.0005 in. and then polished and chrome-plated to a surface smoothness of 10^{-6} in. Two matching pairs of such plate molds were used. A thin coat of a mixture of 10% Dow Silicone 20 mold release

grease, 10% toluene and 80% isopropanol was applied and wiped off after drying. The mold plates were spaced by 0.5 in. wide annealed strips of cellulose acetate milled to a uniform thickness and were held against each other by 10 screws on the perimeter. The spacers were placed first on three sides leaving the top open for pouring the hot araldite, after which the fourth spacer was put in place and the screws were uniformly and suitably tightened. The function of the plastic spacers was to yield in compression as they softened and permit a reduction of thickness matching more or less the volume contraction of araldite during setting. In contrast with metal spacers which had caused surface separation during casting as well as high residual stresses and cracks, the plastic spacers gave excellent sheets of uniform thickness having negligible or annealable stresses. After several castings it was possible to select pairs of 9 in. square sheets with thickness variations no larger than ± 0.0005 in. within each sheet or from each other, which was considerably better than with any commercially available product. Sheets of thickness 0.108, and 0.057 in. were chosen.

Araldite 6060 resin with 30% by weight of phthalic anhydride was mixed at 140°C, filtered through fiberglass cloth and cast in hot molds at 120° ± 5°C and cured at 115°C for 8 hours. The cast sheets were removed cold and were laid on an open paper-covered mold and weighted with a thick rubber sheet for annealing at 140°C for 3 hours followed by cooling at the rate of 5°/h to room temperature.

The residual stress field was produced by "shrink-fitting," a 1 in. disc in a narrower hole bored centrally in each sheet. The disc was machined from the border of the plate (initially 13 x 15 in; finally 9 x 9 in.) to which it was fitted. Both turning of the disc and boring of the hole had

to be done with the greatest care on the most accurate machines to achieve perfect roundness and to prevent chatter-marks and uneven fringe patterns. The interference (0.005 to 0.010 in.) was such as to produce about 8 concentric fringes in reflected light in the 0.108 in. coating and about 5 in the 0.057 in. coating. For the two thicker coatings the discs were cooled in liquid nitrogen and were quickly fitted in the plates which had been heated to about 45°C. The same procedure caused conical buckling in the thinnest coating. Accordingly part of the fringe pattern was frozen in the sheet by forcing in the hole of the hot clamped sheet a tapered round bar ending in a cylindrical portion of the desired diameter. The frozen-in pattern was increased by a residual stress pattern by shrink-fitting the disc. This ensured also sufficient pressure between disc and sheet to prevent separation during unfavorable bending.

The pairs of sheets were finally cemented on both faces of the 0.250 in. thick plates of 24ST aluminum. These plates were square with 9 in. sides and had small protrusions at the corners in the directions of the diagonals permitting the transverse load to be applied exactly at the corners of the square. Transverse pins were fitted in these protrusions, centered on the corners and protruding by 0.125 on each side, so as to support spherical ball bearing through which the transverse loads were applied (Fig. 9). Cementing was done with cold setting araldite in a thick layer on which the well centered 9 in. square sheets were placed and then uniformly weighted so as to expell the excess glue. Curing lasted for a week at room temperature. Lack of uniformity of the glue line unfortunately reduced the high accuracy of the sheet thickness. The coatings had a final thickness of 0.108 ± 0.0015 and 0.0565 ± 0.0015 in.

b. Measurements. Observations were made at normal incidence with the help of a set of 3 full mirrors and a partially reflecting front surface mirror placed in the field of a regular transmission polariscope as shown in the diagram of Fig. 10 and the photograph of Fig. 11. Plane polarized light with a fixed plane of vibration perpendicular to the common plane of incidence of all mirrors was used throughout so as to avoid the depolarization from reflexion at other azimuths. The various isoclinics were obtained by rotating the plate in its plane. The angular position was read on a divided circle below the plate (Fig. 9). Fringe measurements were made to the nearest 0.1 fringe at the plate azimuth making brightest the neighborhood of the point under observation. "Isoclinics" were determined to the nearest 1°, but sometimes contained an uncertainty of ±5° or more. The accuracy of the measurements was purposedly kept at the level of ordinary visual observations without compensator or photometer.

As already mentioned it was found more convenient to express and calculate bending moment and membrane force in terms of the fringe order in the coatings, but with expressions (3) all results may be rewritten in terms of M and N. The fringe order from bending alone could be easily detected in the central expansion-fitted disc which initially was in an isotropic state of compression, hence had a zero fringe. A more accurate method was to measure the radial displacement of the "membrane stress" fringes along the plate diagonals, where membrane and bending directions are parallel. Displacement of the integer membrane fringe n_t to the initial position of the fringe $n_t - 1$ along one diagonal and to $n_t + 1$ along the other indicates a value of n_b equal to 1; displacement of n_t to $n_t - 2$ and $n_t + 2$ a value $n_b = 2$, etc. as shown in Figures 12a-c of the lower coating $(z > 0)$

specially taken in circularly polarized light. For measurements on the opposite side ($z < 0$) the plate was turned over and subjected to the same bending, as if it had never been unloaded. To achieve identical bending in both positions reliance was placed not on the intensity of the corner loads, measured by a dynamometer, but on the plate deflection indicated by a special very sensitive deflectometer spanning one diagonal (Fig. 9). In other words bending was controlled by fixed boundary displacements instead of fixed loads. Consequently any photo-viscoelastic fringe shift would be a relaxation effect, which has been found [29] to be appreciably smaller than the corresponding creep under constant applied loads.

At any point of the plate the major membrane stress is circumferential (shrink fit causes a hoop tension and a radial compression outside the central disc) and the major principal bending plane is everywhere (except near the edges) parallel to the diagonal along which the initially circular fringes contract. For convenience this major diagonal on the lower coating was chosen as the reference direction, hence in the present tests $\gamma_b = 0$, $\alpha = -\gamma_t$ and $\phi_{o2} = -\theta_{o2} + 90$, $\phi_{u2} = -\theta_{u2}$ (6). Figure 13 shows corresponding points in the lower and upper coatings having a membrane "stress" of one fringe with principal direction at an angle $\alpha = 30°$ to the major plane of bending (diagonal at A). The angle from $\sigma_1^t > 0$ to $\sigma_1^b > 0$ in the lower coating is also 30° but is $90°-\alpha = 60°$ in the upper coating.

Measurements were made at points with integer values of n_t from 1 to 4, with a bending moment causing values of n_b of 1 or 2 in the 0.108 in. coating, but only $n_b = 1$ in the 0.057 in. coating to avoid permanent straining, and value of angle α from 0° by tens to 90°. At first a point

of selected values n_t, α was identified on the lower coating by cross-hairs conveniently fixed in a wide ring. Figure 14a shows the cross-hairs at a point with $n_t = 2$ ($n_b = 0$) in plane polarized light at a plate azimuth making its neighborhood brightest. Fig. 14b shows the same point to be on the 30° isoclinic ($\alpha = 30°$). The bending moment causing $n_b = 1$ was then applied and the fringe order n_u at the cross-hairs was estimated at the plate azimuth making its neighborhood brightest (Fig. 15a, $n_u = 1.9$). The angle $\phi_{u2} = -\theta_{u2}$ was found from the plate azimuth making the region of the cross-hairs darkest (Fig. 15b, $\phi_{u2} = 12°$). The bending was then increased to $n_b = 2$ and the new values of n_u and ϕ_{u2} were measured (Fig. 16a; $n_u = 2.8$ and Fig. 16b; $\phi_{u2} = 7°$). After all measurements on the lower coating were completed, the plate was turned around at similar measurements which were made on the upper coating.

Test Results

The results are surprisingly good. The observed total fringe order n_o (above) and n_u (below) and their "principal directions" are shown on Mohr's circle constructions in Figures 17 to 19. As shown in the inset to Fig. 17 the superposition of n_b at an angle α to n_t gives the total fringe order $n_u = NA'$ for the coating below. For other angles α the locus of points A' will be a circle of the same radius n_t with center 0 at a distance $MO = n_b$ from M . Likewise for other values of n_t but identical n_b the total fringe points (A') will lie on concentric circles with 0 as center and with the corresponding n_t as radii, as shown in Figures 17 to 19. The magnitude n_u is found as the distance from N of point A' determined by the angle 2α at 0 .

According to the assumptions made in the present paper the apparent principal direction should be the one at the free surface, which is found (see Fig. 5 for the stresses) by increasing n_b to $n_b H/a = AA''$: the desired direction is given by the angle $ONA'' = 2\phi_{u2}$ (Fig. 17, inset). However, instead of drawing a new set of concentric circles for A'', one has only to take the same distance $NF = A'A'' = n_b \Delta h/a$ to the left of N for all values n_t, and determine $2\phi_{u2}$ as the angle $< OFA'$. This was done in all three Figures 17 to 19. The total fringe order n_{o2} and principal direction ϕ_{o2} of the coating above is found in the same way by starting with an angle $2\alpha - 180$ at 0 (clockwise): corresponding pairs of n_{u2}, n_{o2} are at opposite ends of the same diameter.

In Figures 17 to 19 the experimental points have been plotted by drawing a line through F at angle ϕ_{i2} to FN and taking a length n_i <u>from N to that line</u>. The experimental points have been joined to the theoretical by tail-like segments, whose magnitude and direction indicate the corresponding errors. As can be seen the results are extremely good except when α is about 70° or 80° for the coating below, or about 10° to 20° for the coating above, as was expected from an earlier discussion (Figures 3a, b and 5). Even then the magnitudes n_u, n_o are almost exact, the main error being in the directions ϕ_u, ϕ_o.

A computer program (both program and tabulated results are given in the Appendix) was set up for the calculation of n_o and n_u corresponding to the total stress at mid-thickness, as well as by integration (eq. 11), and of ϕ_{o1}, ϕ_{u1} at the interface; ϕ_{o2}, ϕ_{u2} at the free surfaces; and ϕ_{m1}, ϕ_{m2} at mid-thickness. The directions ϕ_{o2}, ϕ_{u2} at the free surface were always closer to the experimental results. Calculations were made for $n_b = 1$ and

$n_b = 2$ with the 0.108 in. coatings and $n_b = 1$ with the 0.057 in. coating. In both cases the values of n_t extended from 1 to 4.

The same program gave the results of the inverse calculation of n_t, n_b, α from the observed values n_u, n_o, ϕ_u, ϕ_o and compared them with their true or nominal values. Furthermore, the neglected quantity A in Eqs. (17) and (18) and the resulting percentage error in δ^2 was computed at each point. The error was throughout either exactly zero or less than $|0.005|$. The nominal total rotation $\phi_{i2} - \phi_{i1}$ through the coatings below and above and the average value $R_{av} = 2(\phi_{i2} - \phi_{i1})/n_i$ of twice the rotation over the coating thickness to the retardation for a stress equal to the one at mid-thickness were also computed. These values are plotted in Figures 3a, b.

The results of the inverse calculation (n_t, n_b, α form n_u, n_o, θ_{u2}, θ_{u0}) are shown in Figures 20 to 22, where they are compared with their true values. The calculated angle α is taken counterclockwise from the horizontal and the calculated magnitude of n_b is marked on it by an empty circle. The calculated value of n_t is taken along the radius corresponding to the true angle α and marked by a black circle. The calculated points are joined to the exact points by tail-like segments. The results are remarkably good even for angles α of about 70° and 20° where respectively θ_{u2} and θ_{o2} had substantial errors. No systematic pattern of errors is apparent. The absolute errors appear to be only slightly larger for $n_t = n_b = 1$ (both thicknesses) than for higher values, but the relative errors are, of course, much smaller for the higher values of n_t and n_b. The independence of absolute error from the magnitude of n_t and n_b may be the result of a constant source of error, such as the small accuracy of measurement (fringe orders measured to the nearest 0.1 fringe, angles to the nearest 1°), which was purposely chosen so as to simulate practical

testing conditions, or the thin cement layer (about 0.002 in.) which had no "membrane" stress. However, the difference between observed and theoretical total birefringence is largest at angles α around 70° (error in n_u) or 20° (error in n_o), Figures 17-19, and it might be expected that the inverse solution for n_b, n_t might also be less accurate. It would therefore be useful to recognize these cases. As may be seen in Figures 17 to 19 when $\alpha = 70°$ or $\alpha = 20°$ the difference $|n_u - n_o|$ is large and the angle $2|\theta_{u2} - \theta_{o2}| = 2|\phi_{o2} - \phi_{u2}|$ is not zero. For zero angle it is easily found that $\alpha = 0$ or $\alpha = 90°$ so that no rotation occurs and the results should be of the highest accuracy. For $n_u \approx n_o$, α should be close to 45°.

It is true that in the present tests the direction of the bending moment was known (major diagonal) and did not have to be calculated. This calculation may easily be made as explained at the end of the previous paragraph but would not affect the calculated values of n_b, n_t, and α, as the only possible new error would be identical in both directions γ_b and γ_t of M and N and not in their relative angle α.

Conclusions

The tests show that with the proposed method using two birefringent coatings, the principal membrane and bending stress differences can be determined with an accuracy of about 5% to 10% in magnitude and ±2° to 5° in direction. This compares quite favorably with the accuracy (5% and 2°) expected in two-dimensional photoelasticity.

TECHNICAL LIBRARY
BLDG. 313
ABERDEEN PROVING GROUND MD.
STEAP-TL

Acknowledgment

The authors acknowledge gratefully the financial support given for this research partly by the National Science Foundation under Grant G-20259, by the Advanced Research Projects Agency under Contract SD-86, and by the Division of Engineering, Brown University.

Mr. Frank Anrep designed the multiple mirror unit for using reflected polarized light at normal incidence. Mr. Roland Beaulieu made the molding plates and developed the flexible spacers for casting the highly accurate pairs of epoxy sheets. Mr. Roger Paul fitted the discs in the plates, Mr. Graham Brown checked and re-programmed the computations and Mr. Laurenz Hermann photographed the fringe patterns. Without their assistance this report would not have been completed.

References

1. Schumann, W., and Mylonas, C., "On the Separation of Membrane and Bending Stresses in Shells with Two Birefringent Coatings, Report DA-4674/5 of the Division of Applied Mathematics, Brown University, July 1960.

2. Mesnager, M., "Sur la Determination Optique des Tensions Interieures dans les Solides a Trois Dimensions," Comptes Rendus, Paris, Vol. 190, 1930, p. 1249.

3. Oppel, G., "Das polarisationsoptische Schichtverfaren zur Messung der Oberflachenspannungen am beanspruchten Bauteil ohne Model," Z. VDI, Vol. 81, 1937, p. 638.

4. D'Agostino, J., Drucker, D. C., Liu, C. K., and Mylonas, C., "An Analysis of Plastic Behavior of Metals with Bonded Birefringent Plastics," Proc. of the Society for Experimental Stress Analysis, Vol. XII, No. 2, 1955, pp. 115-122.

5. D'Agostino, J., Drucker, D. C., Liu, C. K., and Mylonas, C., "Epoxy Adhesives and Casting Resins as Photoelastic Plastics," Proc. of the Society for Experimental Stress Analysis, Vol. XII, No. 2, 1955, pp. 123-128.

6. Fleury, R., and Zandman, F., "Jauge d'Efforts Photoélastique," Comptes Rendus, Paris, Vol. 238, 1954, p. 1559.

7. Zandman, F., "Analyse des Contraintes par Vernis Photoélastique," Groupement pour l'Avancement des Methodes d'Analyse des Contraintes, Vol. 2, No. 6, 1956, pp. 3-14.

8. Kawata, K., "Analysis of Elastoplastic Behavior of Metals by Means of Photoelastic Coating Method," J. Sci. Res. Inst., Tokyo, Vol. 52, 1958, pp. 17-40.

9. Duffy, J., "Effects of the Thickness of Birefringent Coatings," J. Experimental Mechanics, Vol. 1, No. 3, March 1961, pp. 74-82.

10. Neumann, F., "Die Gesetze der Doppelbrechung des Lichtes in komprimierten oder ungleichformig erwarmten unkrystallinischen Korpern," Abh. d. Kon. Akad. d. Wissenschaften zu Berlin, Pt. II, 1841.

11. Poincare, H., "Théorie Mathematique de la Lumière, Paris, 1882.

12. Drucker, D. C., and Mindlin, R. D., "Stress-Analysis by Three-Dimensional Photoelastic Methods," J. App. Physics, Vol. 11, No. 11, November 1940, pp. 724-732.

13. Jones, R. C. "A New Calculus for the Treatment of Optical Systems, J. Opt. S. A., Parts I, 31 (1941) 488, III 500; IV, 32 (1942) 486; V, 37 (1947) 107; VI 110; VII, 38 (1948) 671; VIII, 46 (1956) 126. Also Hurwitz, H., Jr., and Jones, R. C., Part II, J. Opt. S. A. 31 (1941) 493.

14. Mindlin, R. D., "An Extension of the Photoelastic Method of Stress Measurement to Plates in Transverse Bending," Trans. ASME, Vol. 63, 1941, p. A-187.

15. Drucker, D. C., "The Photoelastic Analysis of Transverse Bending of Plates in the Standard Transmission Polariscope," J. Appl. Mechanics, Trans. ASME, Vol. 64, 1942, pp. A-161 - A-164.

16. Mindlin, R. D., and Goodman, L. E., "The Optical Equations of Three-Dimensional Photoelasticity," J. Appl. Physics, Vol. 20, No. 1, January 1949, pp. 89-95.

17. Ramachandran, G. N., and Ramaseshan, S., "Crystal Optics," Handbook of Physics, (S. Flugge, Editor), Vol. XXV/1, 1-217, Springer, 1961.

18. Shurcliff, W. A., Polarized Light, Harvard Univ. Press, 1962.

19. Aben, H. K., "Photoelastic Phenomena by Uniform Rotation of Principal Axes," Izv. Akad. Nauk. SSSR, Mekh. i Mashinostr. (3), 141-147 (1962).

20. Aben, H. K., "Optical Phenomena in Photoelastic Models by the Rotation of Principal Axes," Exp. Mech. 6 (1), 13-22, 1966.

21. Menges, H. J., "Die Experimentelle Ermittlung Räumlicher Spannungszustände an Durchsichtigen Modellen mit Hilfe des Tyndalleffectes Z. Aug. Math. Mech. 20 (4), 210-7 (1940).

22. Kuske, A., "Einführung in die Spannungsoptik," Wissenschaftliche Verlaggesellschaft M.B.H., Stuttgart (1959).

23. Kayser, R., "Spannungsoptische Untersuchung von allgemeinen Flähentragwerken unter direkter Beobachtung," Dissertation, T. H. Stuttgart (1964).

24. Kuske, A., "L'analyse des Phenomenes optiques en photoelasticite a trois dimensions par la methode du cercle de j," Rev. Franc. de Mec., 9, 49-58 (1964).

25. Aben, H. K., "On the Application of Photoelastic Coatings for the Investigation of Shells," Izv. Akad. Nauk SSSR Mekh. i Mashinostr. 7 (6), 106-111 (1964).

26. Akhmetzyanov, M. Kh., "Application of the Method of Photoelastic Coatings to the Determination of the Stresses and Deformations in Flexible Plates and Shells," Izv. Akad. Nauk. SSSR, Mekh. i Mashinostr., No. 1, 199-201, 1964. NASA Tech. Transl. TTF-220, July 1964.

27. Mylonas, C., to be published.

28. Gilg, B., "Experimentelle und Theoretische Untersuchungen an dunnen Platten," Diss. ETH., Ed. Leeman, Zurich, 1952.

29. Mylonas, C., and Drucker, D. C., "Twisting Stresses in Tape," J. Appl. Mech., Vol. 1, 1961.

30. Wood, A.F.B., "On the Photoelastic Examination of Vibrating Bodies and the Photoelastic Effect in Optically Active Media," J. Mech. Phys. Solids, 8, 26-38 (1960).

31. Mark, R., "A Simple Geometric Method for Analyzing Polarization States in Photoelasticity," AIAA Journal, Vol. 2, No. 1, pp. 149-152, 1964.

32. Ramberg, W., and Miller, J. A., "Determination of Stress-Strain Curve in Shear by Twisting Square Plate," Proc. 1st U. S. Congress App. Mech., pp. 513-519, 1951.

33. Favre, H., and Schumann, W., "A Photoelectric-Interferometric Method to Determine Separately the Principal Stresses in Two-Dimensional States and Possible Applications to Surface and Thermal Stresses," Photoelasticity, Proc. of the Int. Symp. on Photoelasticity, M. M. Frocht, Editor, pp. 3-25, Pergamon Press, 1963.

34. Robert, A. J., and Guillemet, E., "Nouvelle methode d'utilisation de la lumière diffusee en photoélasticimetrie à trois dimensions," Revue Française de Mécanique, Nos 5/5 - 7/8 (1963).

35. Robert, A. J., "New Methods in Photoelasticity," J. of Exp. Mechanics, 7 (4), 224-232, 1967.

mlw

APPENDIX

Computer Program and Tabulated Results

The computer program is given in pages 40-45 and the tabulated results in Tables I (0.108 in. coatings) and II (0.057 in. coatings), pages 46-52 and 53-56 respectively.

In Tables I and II the results are given in sets of 3 lines, each set corresponding to a single point. The first of each set of three lines (Row NOM) gives the actual or nominal values of the fringe order n_t due to membrane stress only (column NT); n_b due to bending only (column NB); the angle α of their principal directions (column ALFA); the total expected fringe orders n_u, n_o (columns NU, NO) below and above and surface principal directions ϕ_u, ϕ_o (columns PU, PO) as calculated by the approximate formulas (12) and (16).

The second row (EXP) of each set of three lines gives under the same columns the experimental values n_u, n_o, ϕ_u, ϕ_o and the inversely calculated values of n_t, n_b and α according to formulas (17, with A = 0), (13), (7) and (14).

The third row (INT) gives the value of the total apparent fringe orders n_u, n_o (columns NU, NO) as found from the integrated form (11a,b). The value of the neglected quantity A computed as in (18) is given in Row INT under column PO; and the percentage error in δ^2 due to the neglect of A is given under column PU. As can be seen both A and the error in δ^2 are either exactly zero (shown by 0.0) or less than $|0.005|$ (shown by 0.00). For $n_b = n_t$, $\alpha = 0$, the value of A is zero but the percentage error in δ^2 is indeterminate (****). The last but one column DF2-1 gives the total

rotation of principal stress in degrees from free surface to interface in coating below (first row) and above (second row). The last column RAV E-3 gives the value $R_{av} \times 10^3$ (radians per fringe) of the average rotation divided by half the total retardation in the coating below (first row) and above (second row).

COMPUTER PROGRAM

```
VEL 02 NOV. 66                                     OS/360   FORTRAN H

        COMPILER OPTIONS - NAME=  MAIN,OPT=00,LINECNT=60,SOURCE,BCD,NOLIST,NODECK,LO

 ISN 0002            DIMENSION  A(2),B(2),C(2),D(2),P(2),E(2),F(2),DF21(2),RAV(2),
                    ?  V(2),U(2),W(2),JTAB(6),XP(2),XNINT(2),SN(2) ,DF22(2)
 ISN 0003            READ(1,1000)  HI,H
 ISN 0004       1000  FORMAT(4F10.5)
 ISN 0005            HO=(HI+H)/2.
 ISN 0006            DO 1423 I=1,6
 ISN 0007       1423  JTAB(I)=0
 ISN 0008            JTAB(1)=1
 ISN 0009            JTAB(5)=1
 ISN 0010            K=0
 ISN 0011            CALL WRITE(HI,H)
               C  THE NEXT CARD MUST BE CHANGED IN THE FINAL PROGRAM
 ISN 0012            JTAB(6)=0
 ISN 0013          1  READ(1,1000,END=1032) SNU,SNO,PU,PO
 ISN 0014            THETAM=2.*(PO-PU)
 ISN 0015            THETAD=ABS(THETAM)
 ISN 0016              THETA=(THETAM*3.14159)/180.0
 ISN 0017            IF(91.0-THETAD) 30,20,20
 ISN 0018         20 IF(THETAD-89.0)  30,40,40
 ISN 0019         30 EM=((SNO**2-SNU**2)/(SNO**2+SNU**2))**2
 ISN 0020            SEM=SQRT(1.0-EM)
 ISN 0021            J=1
 ISN 0022            IF(EM-0.90)  13,13,11
 ISN 0023         13 DEN=1.-(1.-EM*(HO/HI)**2)*((COS(THETA)**2))
 ISN 0024            IL=0
 ISN 0025            DELT2=((1.+SEM*COS(THETA))**2)/DEN
 ISN 0026            DELT=SQRT(DELT2)
 ISN 0027            GO TO 50
 ISN 0028         40 DELT=1.0
 ISN 0029            J=-1
 ISN 0030            GO TO 50
 ISN 0031         11 DELT=HI/HO
 ISN 0032            IL=1
 ISN 0033         50 TEN=SQRT((0.5*(SNO**2+SNU**2))/(1.+((DELT*HO)/HI)**2))
 ISN 0034            BEN=(TEN*DELT*HO)/HI
 ISN 0035            COS2A=(SNU**2-SNO**2)/(4.*TEN*BEN)
 ISN 0036            OV=THETA
 ISN 0037            IF(COS2A-1.) 49,18,18
 ISN 0038         18 COS2A=1.00
 ISN 0039         49 IF(-COS2A-1.) 97,98,98
 ISN 0040         98 COS2A=-1.00
 ISN 0041         97 CONTINUE
 ISN 0042            ALFTR=ARCOS(COS2A)
 ISN 0043            IF(J)  60,61,61
 ISN 0044         61 ALFR=ALFTR
 ISN 0045            GO TO 70
 ISN 0046         60 IF(OV) 62,63,63
 ISN 0047         62 ALFR=ALFTR
 ISN 0048            GO TO 70
 ISN 0049         63 ALFR=-ALFTR
 ISN 0050         70 ALF=(ALFR*180.0)/(2.*3.14159)
 ISN 0051            DH=HI-H
 ISN 0052            TZN=JTAB(1)
 ISN 0053            RHO=(JTAB(6)*3.141592)/90.
 ISN 0054            SIN2A=SIN(RHO)
 ISN 0055            COS2A=COS(RHO)
 ISN 0056            DELT=(JTAB(5)*HI)/(JTAB(1)*HO)
 ISN 0057            A(1)=DELT+COS2A
 ISN 0058            A(2)=DELT-COS2A
```

```
ISN 0059           B(1)=(DELT*H)/HI+COS2A
ISN 0060           B(2)=(DELT*H)/HI-COS2A
ISN 0061           C(1)=(DELT*HO)/HI+COS2A
ISN 0062           C(2)=(DELT*HO)/HI-COS2A
ISN 0063           D(1)=COS2A+DELT
ISN 0064           D(2)=COS2A-DELT
ISN 0065           E(1)=COS2A+(DELT*H)/HI
ISN 0066           E(2)=COS2A-(DELT*H)/HI
ISN 0067           DO 44 I=1,2
            C            HERE 1=U, 2=O
ISN 0068           IF(ABS(SIN2A)-0.005) 89,89,88
ISN 0069        89 XNINT(1)=JTAB(1)+JTAB(5)
ISN 0070           XNINT(2)=JTAB(1)-JTAB(5)
ISN 0071           SN(I)=SQRT((TZN**2)*(C(I)**2+SIN2A**2))
ISN 0072           GO TO 87
ISN 0073        88 CONTINUE
ISN 0074           V(I)=(A(I)+SQRT(A(I)**2+SIN2A**2))/(B(I)+SQRT(B(I)**2+SIN2A**2))
ISN 0075           U(I)=A(I)*SQRT(A(I)**2+SIN2A**2)
ISN 0076           W(I)=B(I)*SQRT(B(I)**2+SIN2A**2)
ISN 0077           SN(I)=SQRT((TZN**2)*(C(I)**2+SIN2A**2))
ISN 0078           V(I)=ABS(V(I))
ISN 0079           IF(ABS(V(I))-0.005) 33,33,32
ISN 0080        33 XNINT(1)=JTAB(1)-JTAB(5)
ISN 0081           XNINT(2)=JTAB(1)+JTAB(5)
ISN 0082           GO TO 87
ISN 0083        32 CONTINUE
ISN 0084           XNINT(I)=(HI/(2.*DELT*DH))*TZN*(U(I)-W(I)+(SIN2A**2)*ALOG(V(I)) )
ISN 0085        87 CONTINUE
ISN 0086           F(I)=ATAN2(SIN2A,E(I))
ISN 0087           P(I)=ATAN2(SIN2A,D(I))
ISN 0088           CALL SIHZ(F(I),RHO,RES,I)
ISN 0089           F(I)=RES
ISN 0090           CALL SIHZ(P(I),RHO,RES,I)
ISN 0091           P(I)=RES
ISN 0092           DF21(I)=P(I)-F(I)
ISN 0093           DF22(I)=(DF21(I)*180.)/3.141592
ISN 0094           P(I)=(P(I)*90.0)/3.14159
ISN 0095           F(I)=(F(I)*90.)/3.14159
ISN 0096           DF22(I)=DF22(I)/2.
ISN 0097        44 CONTINUE
ISN 0098           IF(SNU) 80,81,80
ISN 0099        81 RAV(1)=999999999.9
ISN 0100           GO TO 83
ISN 0101        80 CONTINUE
ISN 0102           RAV(1)=1000.*DF21(1)/SNU
ISN 0103        83 IF(SNO) 84,85,84
ISN 0104        85 RAV(2)=999999999.9
ISN 0105           GO TO 86
ISN 0106        84 CONTINUE
ISN 0107           RAV(2)=1000.0*DF21(2)/SNO
ISN 0108        86  CONTINUE
ISN 0109           DH2=DH**2
ISN 0110           AA=1.-EM-EM*(SIN(THETA)**2)*(DH2/(8.0*HO*HI))**2
ISN 0111           IF(IL) 300,300,301
ISN 0112       301 IF(AA)302,303,303
ISN 0113       303  AC=2.*(SQRT(AA)-SEM)
ISN 0114           GO TO 132
ISN 0115       302  IF(AA+0.001) 130,305,305
ISN 0116       305 AA=0.
ISN 0117           GO TO 130
```

```
ISN 0118       300  CONTINUE
ISN 0119            IF(AA) 130,131,131
ISN 0120       131  AB=(1.+SEM*COS(THETA))**2
ISN 0121            AN=(2.*COS(THETA))*(SQRT(AA)-SEM)
ISN 0122            IF(AB) 54,55,54
ISN 0123        55  AC=-AA
ISN 0124            GO TO 56
ISN 0125        54  AC=AN/AB
ISN 0126        56  AA=AN
ISN 0127            GO TO 132
ISN 0128       130  AC=999999.9
              C THIS NUMBER IS >THAN THATALLOWED BY THE FORMAT AND WILL PRINT AS ***
ISN 0129       132  CONTINUE
ISN 0130            IF(K-14) 91,92,92
ISN 0131        92  WRITE(3,501)
ISN 0132            K=-1
ISN 0133        91  CONTINUE
ISN 0134            IF(JTAB(1)-1) 220,411,220
ISN 0135       411   IF(JTAB(6)-0) 220,210,220
ISN 0136       210  WRITE(3,501)
ISN 0137       220  WRITE(3,502) JTAB(1),JTAB(5),JTAB(6),SN(1),SN(2),P(1),P(2),DF22(1
                   ? ,RAV(1)
ISN 0138       230  WRITE(3,504) TEN,BEN,ALF,SNU,SNO,PU,PO,DF22(2),RAV(2)
ISN 0139       240  WRITE(3,503) XNINT(1),XNINT(2),AC,AA
ISN 0140       501  FORMAT('1',10X,'     NT      NB      ALFA      NU     NO       PU       P
                   ?     DF2-1  RAV E-3')
ISN 0141       502  FORMAT(1HO,10X,'NOM',I4,2X,I4,2X,I6,3X,F4.2,3X,F4.2,2X,F6.2,2X,
                   ? F6.2,3X,F6.2,2X,F6.2)
ISN 0142       503  FORMAT(1H ,10X,'INT ',' --      --       --       ',F4.2,3X,F4.2,3X,F6.2
                   ? 2X,F6.2)
ISN 0143       504  FORMAT(1H ,10X,'EXP ',  F4.2,2X,F4.2,2X,F6.2,2X,F4.2,3X,F4.2,2X,
                   ? F6.2,2X,F6.2,3X,F6.2,2X,F6.2)
ISN 0144            KTAB=JTAB(6)
ISN 0145            CALL  VINPT(JTAB,KTAB)
ISN 0146            K=K+1
ISN 0147            GO TO 1
ISN 0148      1032   STOP
ISN 0149            END
```

```
        COMPILER OPTIONS - NAME=  MAIN,OPT=00,LINECNT=60,SOURCE,BCD,NOLIST,NODECK,LO

 ISN 0002              SUBROUTINE WRITE(HI,H)
 ISN 0003              WRITE(3,600)
 ISN 0004              WRITE(3,601)
 ISN 0005              WRITE(3,602)
 ISN 0006              A=2.*H
 ISN 0007              B=HI-H
 ISN 0008              WRITE(3,603) A,B
 ISN 0009        600   FORMAT('1',/////////////////)
 ISN 0010        601    FORMAT(1H0,10X,'SEPARATION OF MEMBRANE AND BENDING'// 11X,'STRES
                      ? DIFFERENCES IN SHELLS WITH'// 14X,'TWO BIREFRINGENT COATINGS')
 ISN 0011        602    FORMAT(1H0,////////////////////)
 ISN 0012        603    FORMAT(1H0, 10X,'PLATE THICKNESS (INCHES)',F6.4/10X,'COATING THI
                      ?KNESS (INCHES)',F6.4)
 ISN 0013              RETURN
 ISN 0014              END
```

COMPILER OPTIONS - NAME= MAIN,OPT=00,LINECNT=60,SOURCE,BCD,NOLIST,NODECK,LO

```
ISN 0002          SUBROUTINE VINPT(JTAB,KTAB)
ISN 0003          DIMENSION  JTAB(6)
ISN 0004          IF(KTAB-40) 30,31,30
ISN 0005     31   IF(JTAB(1)-4) 32,33,33
ISN 0006     33   JTAB(6)=45
ISN 0007          JTAB(1)=1
ISN 0008           RETURN
ISN 0009     32   JTAB(1)=JTAB(1)+1
ISN 0010          RETURN
ISN 0011     30   IF(KTAB-45) 40,41,40
ISN 0012     41   IF(JTAB(1)-4) 42,43,43
ISN 0013     42   JTAB(1)=JTAB(1)+1
ISN 0014          JTAB(6)=45
ISN 0015          RETURN
ISN 0016     43   JTAB(6)=50
ISN 0017          JTAB(1)=1
ISN 0018          RETURN
ISN 0019     40   CONTINUE
ISN 0020          IF(KTAB-90) 10,11,11
ISN 0021     10   CONTINUE
ISN 0022          GO TO 13
ISN 0023     11   IF(JTAB(1)-4) 13,21,21
ISN 0024     21   JTAB(6)=0
ISN 0025          JTAB(1)=1
ISN 0026          JTAB(5)=JTAB(5)+1
ISN 0027          RETURN
ISN 0028     13   CONTINUE
ISN 0029          JTAB(1)= JTAB(1)+1
ISN 0030          IF(JTAB(1)-5)  997,999,999
ISN 0031    997   RETURN
ISN 0032    999     JTAB(1)=1
ISN 0033     12   JTAB(6)=KTAB+10
ISN 0034          RETURN
ISN 0035          END
```

VEL 02 NOV. 66 OS/360 FORTRAN H

COMPILER OPTIONS - NAME= MAIN,OPT=00,LINECNT=60,SOURCE,BCD,NOLIST,NODECK,LO

```
ISN 0002          SUBROUTINE SIHZ(S1,S2,S3,I)
ISN 0003           IF(I-1) 150,150,151
ISN 0004     150   IF(S2) 152,153,153
ISN 0005     153  IF(S1) 154,155,155
ISN 0006     155  S3=S1
ISN 0007          RETURN
ISN 0008     154   S3=S1+3.14159
ISN 0009          RETURN
ISN 0010     152  IF(S1) 156,157,157
ISN 0011     157  S3=S1-3.14159
ISN 0012          RETURN
ISN 0013     156  S3=S1
ISN 0014          RETURN
ISN 0015     151   IF(S2) 162,163,163
ISN 0016     163  IF(S1) 164,165,165
ISN 0017     165  S3=S1-3.14159
ISN 0018          RETURN
ISN 0019     164  S3=S1
ISN 0020          RETURN
ISN 0021     162  IF(S1) 166,167,167
ISN 0022     167  S3=S1
ISN 0023          RETURN
ISN 0024     166  S3=S1+3.14159
ISN 0025          RETURN
ISN 0026          END
```

TABLE I

TABULATED RESULTS
COATING THICKNESS 0.1079 in.
PLATE THICKNESS 0.2470 in.

	NT	NB	ALFA	NU	NO	PU	PO	DF2-1	RAV E-3
NOM	1	1	0	2.00	0.00	0.0	0.00	0.0	0.0
EXP	1.00	1.00	0.0	2.00	0.0	0.0	-90.00	90.00	******
INT	--	--	--	2.00	0.0	******	0.0		
NOM	2	1	0	3.00	1.00	0.0	-90.00	0.0	0.0
EXP	2.00	1.00	0.0	3.00	1.00	0.0	-90.00	0.0	0.0
INT	--	--	--	3.00	1.00	0.0	0.0		
NOM	3	1	0	4.00	2.00	0.0	-90.00	0.0	0.0
EXP	3.00	1.00	0.0	4.00	2.00	0.0	-90.00	0.0	0.0
INT	--	--	--	4.00	2.00	0.0	0.0		
NOM	4	1	0	5.00	3.00	0.0	-90.00	0.0	0.0
EXP	4.00	1.00	0.0	5.00	3.00	0.0	-90.00	0.0	0.0
INT	--	--	--	5.00	3.00	0.0	0.0		
NOM	1	1	10	1.97	0.35	4.33	-21.60	-1.57	-26.12
EXP	1.19	0.94	8.47	2.10	0.40	5.00	-38.00	41.14	******
INT	--	--	--	1.97	0.39	-0.00	-0.00		
NOM	2	1	10	2.96	1.11	6.06	-65.03	-1.37	-15.99
EXP	2.04	0.97	5.53	3.00	1.10	7.00	-67.00	9.95	315.80
INT	--	--	--	2.96	1.12	0.00	0.00		
NOM	3	1	10	3.95	2.09	6.99	-72.95	-1.15	-10.03
EXP	3.04	0.98	6.73	4.00	2.10	8.00	-73.00	4.16	69.10
INT	--	--	--	3.95	2.09	0.00	0.00		
NOM	4	1	10	4.95	3.08	7.56	-75.43	-0.98	-6.81
EXP	3.98	1.06	9.64	5.00	3.00	7.00	-74.00	2.53	29.45
INT	--	--	--	4.95	3.08	0.00	0.00		
NOM	1	1	20	1.88	0.68	8.63	-25.04	-3.24	-56.57
EXP	1.18	0.92	18.19	2.00	0.70	9.00	-35.00	23.07	******
INT	--	--	--	1.88	0.70	-0.00	-0.00		
NOM	2	1	20	2.84	1.39	12.19	-50.03	-2.80	-33.71
EXP	2.06	0.97	18.18	2.90	1.40	13.00	-51.00	11.49	286.48
INT	--	--	--	2.84	1.40	0.00	0.00		
NOM	3	1	20	3.82	2.32	14.08	-58.64	-2.31	-20.68
EXP	3.02	1.06	19.49	3.90	2.30	15.00	-56.00	6.22	94.47
INT	--	--	--	3.82	2.33	0.00	0.00		
NOM	4	1	20	4.81	3.30	15.24	-62.20	-1.94	-13.83
EXP	3.99	1.08	18.57	4.90	3.20	16.00	-60.00	4.13	45.01
INT	--	--	--	4.81	3.30	0.00	0.00		
NOM	1	1	30	1.73	1.00	12.82	-23.56	-5.13	-94.30
EXP	1.14	1.01	27.62	1.90	1.00	12.00	-28.00	15.06	525.75
INT	--	--	--	1.73	1.01	-0.00	-0.00		
NOM	2	1	30	2.65	1.73	18.47	-40.02	-4.33	-52.17
EXP	2.18	1.04	27.66	2.90	1.80	19.00	-41.00	9.96	193.07
INT	--	--	--	2.65	1.74	0.00	0.00		

	NT	NB	ALFA	NU	NO	PU	PO	DF2-1	RAV E-3
NOM	3	1	30	3.61	2.65	21.41	-47.16	-3.49	-32.92
EXP	3.09	0.96	28.72	3.70	2.70	22.00	-48.00	6.44	83.27
INT	--	--	--	3.61	2.65	0.00	0.00		
NOM	4	1	30	4.58	3.61	23.18	-50.68	-2.88	-21.83
EXP	4.07	0.93	30.14	4.60	3.70	24.00	-51.00	4.63	43.72
INT	--	--	--	4.58	3.61	0.00	0.00		
NOM	1	1	40	1.53	1.29	16.84	-20.53	-7.44	162.24
EXP	1.03	1.03	39.09	1.60	1.30	16.50	-21.00	10.50	281.89
INT	--	--	--	1.54	1.29	-0.00	-0.00		
NOM	2	1	40	2.39	2.07	25.01	-32.05	-6.03	-84.24
EXP	2.08	1.01	38.64	2.50	2.10	25.00	-33.00	7.93	131.89
INT	--	--	--	2.39	2.08	0.00	0.00		
NOM	3	1	40	3.32	2.99	29.15	-37.58	-4.66	-49.28
EXP	2.96	0.93	38.52	3.30	2.90	30.00	-38.00	5.73	68.94
INT	--	--	--	3.33	3.00	0.00	0.00		
NOM	4	1	40	4.29	3.95	31.55	-40.60	-3.73	-30.27
EXP	3.95	1.12	39.64	4.30	3.90	30.00	-40.00	4.39	39.27
INT	--	--	--	4.29	3.95	0.00	0.00		
NOM	1	1	45	1.41	1.41	18.74	-18.74	-8.84	205.72
EXP	1.12	0.99	45.00	1.50	1.50	20.00	-21.00	8.84	205.72
INT	--	--	--	1.42	1.42	0.0	0.0		
NOM	2	1	45	2.24	2.24	28.45	-28.45	-6.96	105.61
EXP	2.06	1.03	45.00	2.30	2.30	29.00	-28.00	6.96	105.61
INT	--	--	--	2.24	2.24	0.0	0.0		
NOM	3	1	45	3.16	3.16	33.25	-33.25	-5.22	-58.74
EXP	3.00	0.98	46.54	3.10	3.20	33.00	-34.00	5.22	56.90
INT	--	--	--	3.17	3.17	0.00	0.00		
NOM	4	1	45	4.12	4.12	35.97	-35.97	-4.09	-34.85
EXP	3.96	1.05	45.00	4.10	4.10	35.00	-36.00	4.09	34.85
INT	--	--	--	4.13	4.13	0.0	0.0		
NOM	1	1	50	1.29	1.53	20.53	-16.84	-10.50	261.75
EXP	1.04	1.09	48.82	1.40	1.60	18.00	-18.00	7.44	162.24
INT	--	--	--	1.29	1.54	-0.00	-0.00		
NOM	2	1	50	2.07	2.39	32.05	-25.01	-7.93	138.48
EXP	1.94	0.94	50.11	2.00	2.30	33.00	-25.00	6.03	91.57
INT	--	--	--	2.08	2.39	0.00	0.00		
NOM	3	1	50	2.99	3.32	37.58	-29.15	-5.73	-66.64
EXP	2.98	1.03	49.44	3.00	3.30	37.00	-29.00	4.66	49.28
INT	--	--	--	3.00	3.33	0.00	0.00		
NOM	4	1	50	3.95	4.29	40.60	-31.55	-4.39	-38.29
EXP	3.99	0.94	48.14	4.00	4.20	41.00	-32.00	3.73	30.99
INT	--	--	--	3.95	4.29	0.00	0.00		
NOM	1	1	60	1.00	1.73	23.56	-12.82	-15.06	525.75
EXP	1.10	0.95	61.14	1.00	1.80	26.00	-15.00	5.13	99.54
INT	--	--	--	1.01	1.73	-0.00	-0.00		

	NT	NB	ALFA	NU	NO	PU	PO	DF2-1	RAV E-3
NOM	2	1	60	1.73	2.65	40.02	-18.47	-9.96	193.07
EXP	2.14	0.98	61.59	1.80	2.80	42.00	-19.00	4.33	54.04
INT	--	--	--	1.74	2.65	0.00	0.00		
NOM	3	1	60	2.65	3.61	47.16	-21.41	-6.44	-83.27
EXP	3.04	0.93	60.02	2.70	3.60	49.00	-21.00	3.49	33.83
INT	--	--	--	2.65	3.61	0.00	0.00		
NOM	4	1	60	3.61	4.58	50.68	-23.18	-4.63	-43.72
EXP	4.11	1.00	60.31	3.70	4.70	51.00	-23.00	2.88	21.36
INT	--	--	--	3.61	4.58	0.00	0.00		
NOM	1	1	70	0.68	1.88	25.04	-8.63	-23.07	******
EXP	1.18	0.78	76.43	0.60	1.90	43.00	-10.00	3.24	59.55
INT	--	--	--	0.70	1.88	0.00	0.00		
NOM	2	1	70	1.39	2.84	50.03	-12.19	-11.49	286.48
EXP	2.05	0.99	71.26	1.40	2.90	51.00	-12.00	2.80	33.71
INT	--	--	--	1.40	2.84	0.00	0.00		
NOM	3	1	70	2.32	3.82	58.64	-14.08	-6.22	-94.47
EXP	3.05	0.98	73.14	2.30	3.90	60.00	-14.00	2.31	20.68
INT	--	--	--	2.33	3.82	0.00	0.00		
NOM	4	1	70	3.30	4.81	62.20	-15.24	-4.13	-45.01
EXP	3.95	1.01	71.72	3.20	4.80	62.00	-15.00	1.94	14.12
INT	--	--	--	3.30	4.81	0.00	0.00		
NOM	1	1	80	0.35	1.97	21.60	-4.33	-41.14	******
EXP	1.16	0.89	78.01	0.50	2.00	40.00	-5.00	1.57	27.43
INT	--	--	--	0.39	1.97	-0.00	-0.00		
NOM	2	1	80	1.11	2.96	65.03	-6.06	-9.95	315.80
EXP	2.04	0.96	85.73	1.10	3.00	70.00	-6.00	1.37	15.99
INT	--	--	--	1.12	2.96	0.00	0.00		
NOM	3	1	80	2.09	3.95	72.95	-6.99	-4.16	-69.10
EXP	3.04	0.99	82.31	2.10	4.00	73.00	-7.00	1.15	10.03
INT	--	--	--	2.09	3.95	0.00	0.00		
NOM	4	1	80	3.08	4.95	75.43	-7.56	-2.53	-29.45
EXP	3.99	1.03	82.82	3.00	5.00	76.00	-7.00	0.98	6.81
INT	--	--	--	3.08	4.95	0.00	0.00		
NOM	1	1	90	0.00	2.00	0.00	0.00	-90.00	******
EXP	1.00	1.00	90.00	0.0	2.00	0.0	0.0	0.0	0.0
INT	--	--	--	2.00	0.0	0.0	0.0		
NOM	2	1	90	1.00	3.00	90.00	0.00	-0.00	-0.00
EXP	2.00	1.00	90.00	1.00	3.00	90.00	0.0	0.0	0.0
INT	--	--	--	3.00	1.00	0.0	0.0		
NOM	3	1	90	2.00	4.00	90.00	0.00	-0.00	-0.00
EXP	3.00	1.00	90.00	2.00	4.00	90.00	0.0	0.00	0.00
INT	--	--	--	4.00	2.00	0.0	0.0		
NOM	4	1	90	3.00	5.00	90.00	0.00	0.0	0.0
EXP	4.00	1.00	90.00	3.00	5.00	90.00	0.0	0.00	0.00
INT	--	--	--	5.00	3.00	0.0	0.0		

	NT	NB	ALFA	NU	NO	PU	PO	DF2-1	RAV E-3
NOM	1	2	0	3.00	1.00	0.0	0.00	0.0	0.0
EXP	1.00	2.00	0.0	3.00	1.00	0.0	-0.0	0.0	0.0
INT	--	--	--	3.00	1.00	0.0	0.0		
NOM	2	2	0	4.00	0.00	0.0	0.00	0.0	0.0
EXP	2.00	2.00	0.0	4.00	0.0	0.0	-90.00	90.00	******
INT	--	--	--	4.00	0.0	******	0.0		
NOM	3	2	0	5.00	1.00	0.0	-90.00	0.0	0.0
EXP	3.00	2.00	0.0	5.00	1.00	0.0	-90.00	0.0	0.0
INT	--	--	--	5.00	1.00	0.0	0.0		
NOM	4	2	0	6.00	2.00	0.0	-90.00	0.0	0.0
EXP	4.00	2.00	0.0	6.00	2.00	0.0	-90.00	0.0	0.0
INT	--	--	--	6.00	2.00	0.0	0.0		
NOM	1	2	10	2.96	1.11	2.75	-5.79	-1.42	-15.98
EXP	1.08	2.06	9.78	3.10	1.10	3.00	-6.00	12.76	404.82
INT	--	--	--	2.96	1.12	-0.00	-0.00		
NOM	2	2	10	3.94	0.69	4.33	-21.60	-1.57	-13.72
EXP	2.02	2.02	8.53	4.00	0.60	5.00	-42.00	41.14	******
INT	--	--	--	3.94	0.77	-0.00	0.08		
NOM	3	2	10	4.93	1.31	5.35	-50.81	-1.49	-10.43
EXP	3.09	1.92	3.38	5.00	1.20	6.00	-57.00	21.33	620.52
INT	--	--	--	4.93	1.34	0.00	0.00		
NOM	4	2	10	5.92	2.23	6.06	-65.03	-1.37	-7.99
EXP	4.03	2.00	5.60	6.00	2.10	6.50	-66.00	9.95	165.42
INT	--	--	--	5.92	2.24	0.00	0.00		
NOM	1	2	20	2.84	1.39	5.39	-9.62	-2.90	-34.91
EXP	1.05	2.02	20.37	2.90	1.40	6.00	-10.00	13.26	330.69
INT	--	--	--	2.84	1.40	-0.00	-0.00		
NOM	2	2	20	3.76	1.37	8.63	-25.04	-3.24	-29.01
EXP	2.13	2.02	19.70	3.90	1.40	9.00	-27.00	23.07	575.33
INT	--	--	--	3.76	1.41	-0.00	-0.00		
NOM	3	2	20	4.71	1.95	10.73	-40.43	-3.07	-21.85
EXP	3.15	1.98	17.45	4.90	1.90	11.00	-43.00	17.15	315.08
INT	--	--	--	4.71	1.98	0.00	0.00		
NOM	4	2	20	5.68	2.78	12.19	-50.03	-2.80	-17.00
EXP	4.07	1.98	19.24	5.75	2.80	12.50	-50.00	11.49	143.24
INT	--	--	--	5.68	2.80	0.00	0.00		
NOM	1	2	30	2.65	1.73	7.78	-11.17	-4.51	-56.26
EXP	1.10	2.04	28.29	2.80	1.70	7.00	-13.00	10.91	224.04
INT	--	--	--	2.65	1.74	-0.00	-0.00		
NOM	2	2	30	3.46	2.00	12.82	-23.56	-5.13	-51.19
EXP	2.07	1.96	29.72	3.50	2.00	13.00	-25.00	15.06	262.88
INT	--	--	--	3.47	2.02	-0.00	-0.00		
NOM	3	2	30	4.36	2.65	16.16	-33.45	-4.81	-39.07
EXP	2.98	1.93	29.70	4.30	2.60	17.50	-33.00	12.74	171.04
INT	--	--	--	4.36	2.67	0.00	0.00		

	NT	NB	ALFA	NU	NO	PU	PO	DF2-1	RAV E-3
NOM	4	2	30	5.29	3.46	18.47	-40.02	-4.33	-29.10
EXP	3.99	1.93	30.68	5.20	3.50	19.00	-40.00	9.96	99.29
INT	--	--	--	5.30	3.48	0.00	0.00		
NOM	1	2	40	2.39	2.07	9.75	-11.01	-6.34	-88.49
EXP	1.05	2.06	38.84	2.50	2.10	10.00	-11.00	8.46	140.67
INT	--	--	--	2.39	2.08	-0.00	-0.00		
NOM	2	2	40	3.06	2.57	16.84	-20.53	-7.44	-86.53
EXP	2.07	1.89	40.90	3.00	2.60	18.00	-22.00	10.50	140.94
INT	--	--	--	3.07	2.59	-0.00	-0.00		
NOM	3	2	40	3.88	3.30	21.68	-27.38	-6.86	-59.87
EXP	3.09	1.89	37.87	4.00	3.20	23.00	-28.50	9.41	102.61
INT	--	--	--	3.89	3.32	0.00	0.00		
NOM	4	2	40	4.77	4.15	25.01	-32.05	-6.03	-43.88
EXP	4.06	1.75	37.82	4.80	4.00	27.00	-34.00	7.93	69.24
INT	--	--	--	4.78	4.16	0.00	0.00		
NOM	1	2	45	2.24	2.24	10.49	-10.49	-7.36	116.75
EXP	1.03	1.95	45.00	2.20	2.20	12.00	-10.00	7.36	116.75
INT	--	--	--	2.24	2.24	0.0	0.0		
NOM	2	2	45	2.83	2.83	18.74	-18.74	-8.84	102.86
EXP	2.07	2.10	44.03	3.00	2.90	19.00	-18.00	8.84	106.41
INT	--	--	--	2.84	2.84	-0.00	-0.00		
NOM	3	2	45	3.61	3.61	24.50	-24.50	-8.06	-80.34
EXP	3.07	1.78	45.93	3.50	3.60	27.00	-26.00	8.06	78.11
INT	--	--	--	3.62	3.62	0.00	0.00		
NOM	4	2	45	4.47	4.47	28.45	-28.45	-6.96	-55.21
EXP	3.97	1.90	45.00	4.40	4.40	29.00	-29.00	6.96	55.21
INT	--	--	--	4.48	4.48	0.0	0.0		
NOM	1	2	50	2.07	2.39	11.01	-9.75	-8.46	140.67
EXP	0.93	2.05	50.07	2.10	2.40	10.00	-9.00	6.34	92.18
INT	--	--	--	2.08	2.39	-0.00	-0.00		
NOM	2	2	50	2.57	3.06	20.53	-16.84	-10.50	140.94
EXP	1.97	2.00	49.09	2.60	3.00	20.00	-17.00	7.44	86.53
INT	--	--	--	2.59	3.07	-0.00	-0.00		
NOM	3	2	50	3.30	3.88	27.38	-21.68	-9.41	-99.50
EXP	3.10	1.86	50.40	3.30	3.90	28.00	-24.00	6.86	61.41
INT	--	--	--	3.32	3.89	0.00	0.00		
NOM	4	2	50	4.15	4.77	32.05	-25.01	-7.93	-65.94
EXP	4.02	1.93	49.12	4.20	4.70	33.00	-25.00	6.03	44.81
INT	--	--	--	4.16	4.78	0.00	0.00		
NOM	1	2	60	1.73	2.65	11.17	-7.78	-10.91	224.04
EXP	0.95	2.05	62.21	1.70	2.70	10.00	-7.00	4.51	58.34
INT	--	--	--	1.74	2.65	-0.00	-0.00		
NOM	2	2	60	2.00	3.46	23.56	-12.82	-15.06	262.88
EXP	2.07	1.96	60.28	2.00	3.50	25.00	-13.00	5.13	51.19
INT	--	--	--	2.02	3.47	-0.00	-0.00		

	NT	NB	ALFA	NU	NO	PU	PO	DF2-1	RAV E-3
NOM	3	2	60	2.65	4.36	33.45	-16.16	-12.74	171.04
EXP	3.00	1.91	60.41	2.60	4.30	34.00	-17.00	4.81	39.07
INT	--	--	--	2.67	4.36	0.00	0.00		
NOM	4	2	60	3.46	5.29	40.02	-18.47	-9.96	-99.29
EXP	4.01	1.88	59.66	3.50	5.20	42.00	-18.00	4.33	29.10
INT	--	--	--	3.48	5.30	0.00	0.00		
NOM	1	2	70	1.39	2.84	9.62	-5.39	-13.26	356.13
EXP	1.19	1.91	68.89	1.30	2.90	15.00	-5.00	2.90	34.91
INT	--	--	--	1.40	2.84	-0.00	-0.00		
NOM	2	2	70	1.37	3.76	25.04	-8.63	-23.07	619.58
EXP	2.12	1.99	71.65	1.30	3.90	26.00	-10.00	3.24	29.01
INT	--	--	--	1.41	3.76	-0.00	-0.00		
NOM	3	2	70	1.95	4.71	40.43	-10.73	-17.15	299.33
EXP	3.08	2.00	70.23	2.00	4.80	41.00	-11.00	3.07	22.30
INT	--	--	--	1.98	4.71	0.00	0.00		
NOM	4	2	70	2.78	5.68	50.03	-12.19	-11.49	138.30
EXP	4.07	1.97	69.29	2.90	5.70	49.00	-13.00	2.80	17.15
INT	--	--	--	2.80	5.68	0.00	0.00		
NOM	1	2	80	1.11	2.96	5.79	-2.75	-12.76	445.30
EXP	1.07	1.96	80.81	1.00	3.00	5.00	-4.00	1.42	16.51
INT	--	--	--	1.12	2.96	-0.00	-0.00		
NOM	2	2	80	0.69	3.94	21.60	-4.33	-41.14	******
EXP	2.27	1.74	85.92	0.60	4.00	40.00	-5.00	1.57	13.72
INT	--	--	--	0.77	3.94	-0.00	-0.00		
NOM	3	2	80	1.31	4.93	50.81	-5.35	-21.33	531.87
EXP	3.13	1.92	81.76	1.40	5.00	54.00	-6.00	1.49	10.43
INT	--	--	--	1.34	4.93	0.00	0.00		
NOM	4	2	80	2.23	5.92	65.03	-6.06	-9.95	173.69
EXP	3.99	2.02	86.27	2.00	6.00	68.00	-6.00	1.37	7.99
INT	--	--	--	2.24	5.92	0.00	0.00		
NOM	1	2	90	1.00	3.00	0.00	0.00	-0.00	-0.00
EXP	1.00	2.00	90.00	1.00	3.00	0.0	0.0	0.00	0.00
INT	--	--	--	3.00	1.00	0.0	0.0		
NOM	2	2	90	0.00	4.00	0.00	0.00	-90.00	******
EXP	2.00	2.00	90.00	0.0	4.00	0.0	0.0	0.0	0.0
INT	--	--	--	4.00	0.0	0.0	0.0		
NOM	3	2	90	1.00	5.00	90.00	0.00	-0.00	-0.02
EXP	3.00	2.00	90.00	1.00	5.00	90.00	0.0	0.0	0.0
INT	--	--	--	5.00	1.00	0.0	0.0		
NOM	4	2	90	2.00	6.00	90.00	0.00	-0.00	-0.00
EXP	4.00	2.00	90.00	2.00	6.00	90.00	0.0	0.0	0.0
INT	--	--	--	6.00	2.00	0.0	0.0		

TABLE II

TABULATED RESULTS
COATING THICKNESS 0.0570 in.
PLATE THICKNESS 0.2470 in.

	NT	NB	ALFA	NU	NO	PU	PO	DF2-1	RAV E-3
NOM	1	1	0	2.00	0.00	0.0	0.00	0.0	0.0
EXP	1.00	1.00	0.0	2.00	0.0	0.0	0.0	90.00	******
INT	--	--	--	2.00	0.0	0.0	0.0		
NOM	2	1	0	3.00	1.00	0.0	-90.00	0.0	0.0
EXP	2.00	1.00	0.0	3.00	1.00	0.0	-90.00	0.0	0.0
INT	--	--	--	3.00	1.00	0.0	0.0		
NOM	3	1	0	4.00	2.00	0.0	-90.00	0.0	0.0
EXP	3.00	1.00	0.0	4.00	2.00	0.0	-90.00	0.0	0.0
INT	--	--	--	4.00	2.00	0.0	0.0		
NOM	4	1	0	5.00	3.00	0.0	-90.00	0.0	0.0
EXP	4.00	1.00	0.0	5.00	3.00	0.0	-90.00	0.0	0.0
INT	--	--	--	5.00	3.00	0.0	0.0		
NOM	1	1	10	1.97	0.35	4.57	-27.04	-0.96	-15.88
EXP	1.14	0.99	9.99	2.10	0.40	5.00	-38.00	28.16	******
INT	--	--	--	1.97	0.36	-0.00	-0.00		
NOM	2	1	10	2.96	1.11	6.29	-67.66	-0.84	-9.80
EXP	2.03	1.00	7.66	3.00	1.10	5.00	-71.00	6.00	190.51
INT	--	--	--	2.96	1.12	0.00	0.00		
NOM	3	1	10	3.95	2.09	7.18	-73.92	-0.71	-6.16
EXP	3.03	1.02	10.27	4.00	2.10	8.00	-72.00	2.54	42.24
INT	--	--	--	3.95	2.09	0.00	0.00		
NOM	4	1	10	4.95	3.08	7.73	-75.99	-0.60	-4.28
EXP	3.93	1.03	11.32	4.90	3.00	7.00	-75.00	1.55	18.08
INT	--	--	--	4.95	3.08	0.00	0.00		
NOM	1	1	20	1.88	0.68	9.11	-28.37	-1.97	-36.22
EXP	1.10	0.95	22.53	1.90	0.80	9.00	-35.00	14.56	635.25
INT	--	--	--	1.88	0.69	-0.00	-0.00		
NOM	2	1	20	2.84	1.39	12.65	-52.50	-1.72	-21.42
EXP	2.05	0.92	21.13	2.80	1.50	12.00	-55.00	7.12	165.60
INT	--	--	--	2.84	1.39	0.00	0.00		
NOM	3	1	20	3.82	2.32	14.48	-59.97	-1.42	-13.06
EXP	2.97	1.03	20.69	3.80	2.30	14.00	-59.00	3.84	58.21
INT	--	--	--	3.82	2.33	0.00	0.00		
NOM	4	1	20	4.81	3.30	15.58	-63.06	-1.20	-9.07
EXP	3.85	0.94	20.36	4.60	3.20	16.50	-62.00	2.54	27.73
INT	--	--	--	4.81	3.30	0.00	0.00		
NOM	1	1	30	1.73	1.00	13.58	-25.78	-3.13	-60.61
EXP	1.19	0.84	27.95	1.80	1.00	16.00	-35.00	9.30	324.68
INT	--	--	--	1.73	1.00	0.00	0.00		
NOM	2	1	30	2.65	1.73	19.19	-41.91	-2.66	-34.44
EXP	1.97	1.02	26.93	2.70	1.60	13.00	-48.00	6.18	134.79
INT	--	--	--	2.65	1.74	0.00	0.00		

	NT	NB	ALFA	NU	NO	PU	PO	DF2-1	RAV E-3
NOM	3	1	30	3.61	2.65	22.02	-48.43	-2.15	-20.84
EXP	3.11	0.84	30.29	3.60	2.80	26.00	-48.00	3.98	49.64
INT	--	--	--	3.61	2.65	0.00	0.00		
NOM	4	1	30	4.58	3.61	23.69	-51.60	-1.77	-13.45
EXP	4.02	0.96	28.99	4.60	3.60	25.00	-51.00	2.86	27.74
INT	--	--	--	4.58	3.61	0.00	0.00		
NOM	1	1	40	1.53	1.29	17.94	-22.08	-4.54	105.59
EXP	1.16	0.79	40.61	1.50	1.30	24.00	-27.00	6.43	172.66
INT	--	--	--	1.53	1.29	0.00	0.00		
NOM	2	1	40	2.39	2.07	26.04	-33.45	-3.72	-54.07
EXP	1.99	1.05	40.38	2.40	2.10	25.00	-33.00	4.91	81.56
INT	--	--	--	2.39	2.08	0.00	0.00		
NOM	3	1	40	3.32	2.99	29.98	-38.64	-2.87	-30.40
EXP	2.98	1.02	40.55	3.30	3.00	30.00	-38.00	3.54	41.18
INT	--	--	--	3.32	2.99	0.00	0.00		
NOM	4	1	40	4.29	3.95	32.23	-41.43	-2.30	-18.68
EXP	4.05	0.92	40.21	4.30	4.00	33.00	-42.00	2.71	23.64
INT	--	--	--	4.29	3.95	0.00	0.00		
NOM	1	1	45	1.41	1.41	20.05	-20.05	-5.40	134.70
EXP	1.07	0.90	45.00	1.40	1.40	22.50	-22.50	5.40	134.71
INT	--	--	--	1.42	1.42	-0.00	-0.00		
NOM	2	1	45	2.24	2.24	29.65	-29.65	-4.30	-68.15
EXP	2.04	0.84	45.00	2.20	2.20	32.00	-32.00	4.30	68.15
INT	--	--	--	2.24	2.24	0.0	0.0		
NOM	3	1	45	3.16	3.16	34.20	-34.20	-3.22	-35.13
EXP	3.09	0.84	45.00	3.20	3.20	36.00	-36.00	3.22	35.13
INT	--	--	--	3.16	3.16	0.0	0.0		
NOM	4	1	45	4.12	4.12	36.73	-36.73	-2.53	-21.51
EXP	4.01	0.84	45.00	4.10	4.10	38.00	-38.00	2.53	21.51
INT	--	--	--	4.12	4.12	0.0	0.0		
NOM	1	1	50	1.29	1.53	22.08	-17.94	-6.43	172.66
EXP	1.17	0.77	49.45	1.30	1.50	27.00	-25.00	4.54	105.59
INT	--	--	--	1.29	1.53	0.00	0.00		
NOM	2	1	50	2.07	2.39	33.45	-26.04	-4.91	-85.64
EXP	1.93	1.07	51.15	2.00	2.40	32.00	-25.00	3.72	54.07
INT	--	--	--	2.08	2.39	0.00	0.00		
NOM	3	1	50	2.99	3.32	38.64	-29.98	-3.54	-39.85
EXP	3.03	1.03	47.93	3.10	3.30	39.00	-29.00	2.87	30.40
INT	--	--	--	2.99	3.32	0.00	0.00		
NOM	4	1	50	3.95	4.29	41.43	-32.23	-2.71	-23.64
EXP	4.03	0.98	49.51	4.00	4.30	41.00	-33.00	2.30	18.68
INT	--	--	--	3.95	4.29	0.00	0.00		
NOM	1	1	60	1.00	1.73	25.78	-13.58	-9.30	324.68
EXP	1.13	0.87	60.84	1.00	1.75	30.00	-18.00	3.13	62.34
INT	--	--	--	1.00	1.73	0.00	0.00		

	NT	NB	ALFA	NU	NO	PU	PO	DF2-1	RAV E-3
NOM	2	1	60	1.73	2.65	41.91	-19.19	-6.18	119.82
EXP	2.06	0.87	59.64	1.80	2.60	45.00	-20.00	2.66	35.76
INT	--	--	--	1.74	2.65	0.00	0.00		
NOM	3	1	60	2.65	3.61	48.43	-22.02	-3.98	-51.48
EXP	3.02	1.01	58.90	2.70	3.60	47.00	-23.00	2.15	20.84
INT	--	--	--	2.65	3.61	0.00	0.00		
NOM	4	1	60	3.61	4.58	51.60	-23.69	-2.86	-27.74
EXP	4.02	0.96	61.01	3.60	4.60	52.00	-24.00	1.77	13.45
INT	--	--	--	3.61	4.58	0.00	0.00		
NOM	1	1	70	0.68	1.88	28.37	-9.11	-14.56	677.60
EXP	1.15	0.88	69.57	0.75	1.90	35.00	-14.00	1.97	36.22
INT	--	--	--	0.69	1.88	0.00	0.00		
NOM	2	1	70	1.39	2.84	52.50	-12.65	-7.12	191.08
EXP	2.04	0.94	75.77	1.30	2.90	59.00	-12.00	1.72	20.68
INT	--	--	--	1.39	2.84	0.00	0.00		
NOM	3	1	70	2.32	3.82	59.97	-14.48	-3.84	-58.21
EXP	3.10	1.03	73.59	2.30	4.00	59.00	-17.00	1.42	12.41
INT	--	--	--	2.33	3.82	0.00	0.00		
NOM	4	1	70	3.30	4.81	63.06	-15.58	-2.54	-25.35
EXP	4.14	1.21	64.67	3.50	5.00	60.00	-14.00	1.20	8.35
INT	--	--	--	3.30	4.81	0.00	0.00		
NOM	1	1	80	0.35	1.97	27.04	-4.57	-28.16	******
EXP	1.09	0.97	76.37	0.50	2.00	35.00	-7.00	0.96	16.68
INT	--	--	--	0.36	1.97	-0.00	-0.00		
NOM	2	1	80	1.11	2.96	67.66	-6.29	-6.00	209.56
EXP	1.98	1.04	83.51	1.00	3.00	70.00	-6.00	0.84	9.80
INT	--	--	--	1.12	2.96	0.00	0.00		
NOM	3	1	80	2.09	3.95	73.92	-7.18	-2.54	-42.24
EXP	3.04	1.00	81.75	2.10	4.00	73.00	-9.00	0.71	6.16
INT	--	--	--	2.09	3.95	0.00	0.00		
NOM	4	1	80	3.08	4.95	75.99	-7.73	-1.55	-17.50
EXP	4.03	1.04	78.36	3.10	5.00	74.00	-8.00	0.60	4.19
INT	--	--	--	3.08	4.95	0.00	0.00		
NOM	1	1	90	0.00	2.00	0.00	0.00	-90.00	******
EXP	1.00	1.00	90.00	0.0	2.00	0.0	0.0	0.0	0.0
INT	--	--	--	2.00	0.0	0.0	0.0		
NOM	2	1	90	1.00	3.00	90.00	0.00	-0.00	-0.00
EXP	2.00	1.00	90.00	1.00	3.00	90.00	-0.0	0.0	0.0
INT	--	--	--	3.00	1.00	0.0	0.0		
NOM	3	1	90	2.00	4.00	90.00	0.00	-0.00	-0.00
EXP	3.00	1.00	90.00	2.00	4.00	90.00	-0.0	0.00	0.00
INT	--	--	--	4.00	2.00	0.0	0.0		
NOM	4	1	90	3.00	5.00	90.00	0.00	0.0	0.0
EXP	4.00	1.00	90.00	3.00	5.00	90.00	-0.0	0.0	0.0
INT	--	--	--	5.00	3.00	0.0	0.0		

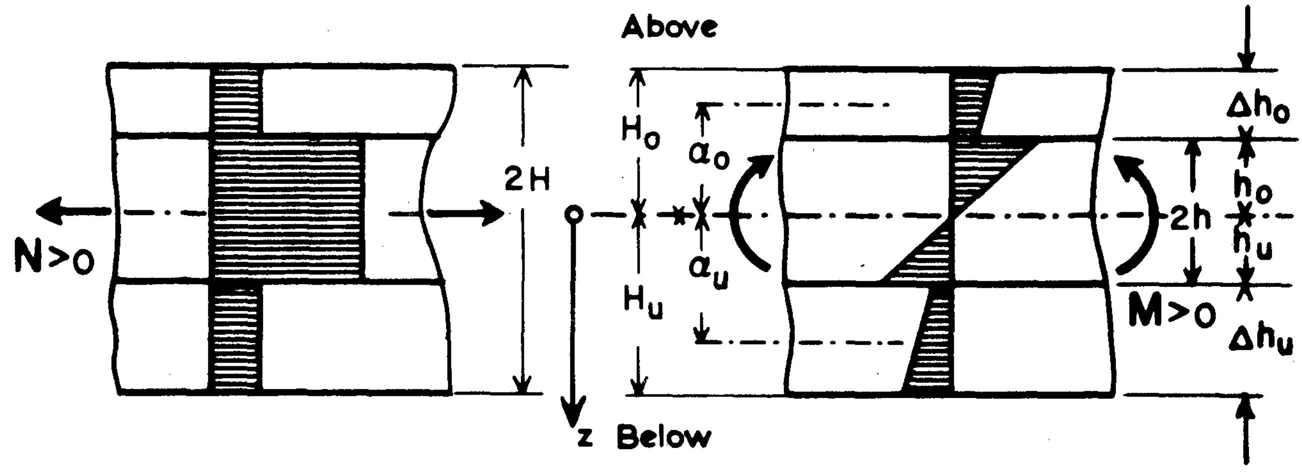

FIG. 1 DOUBLY COATED SHELL IN SIMPLE TENSION AND IN PURE BENDING.

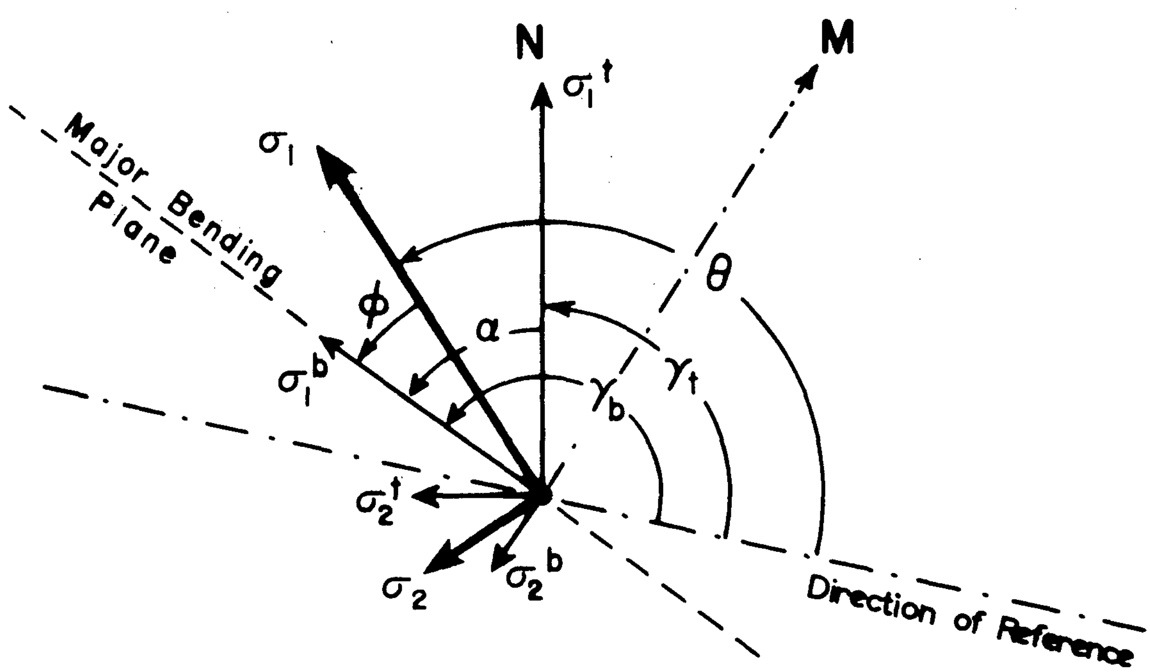

FIG. 2 PRINCIPAL DIRECTIONS OF MEMBRANE, BENDING, AND TOTAL STRESS IN THE LOWER COATING, SEEN FROM BELOW Z > O.

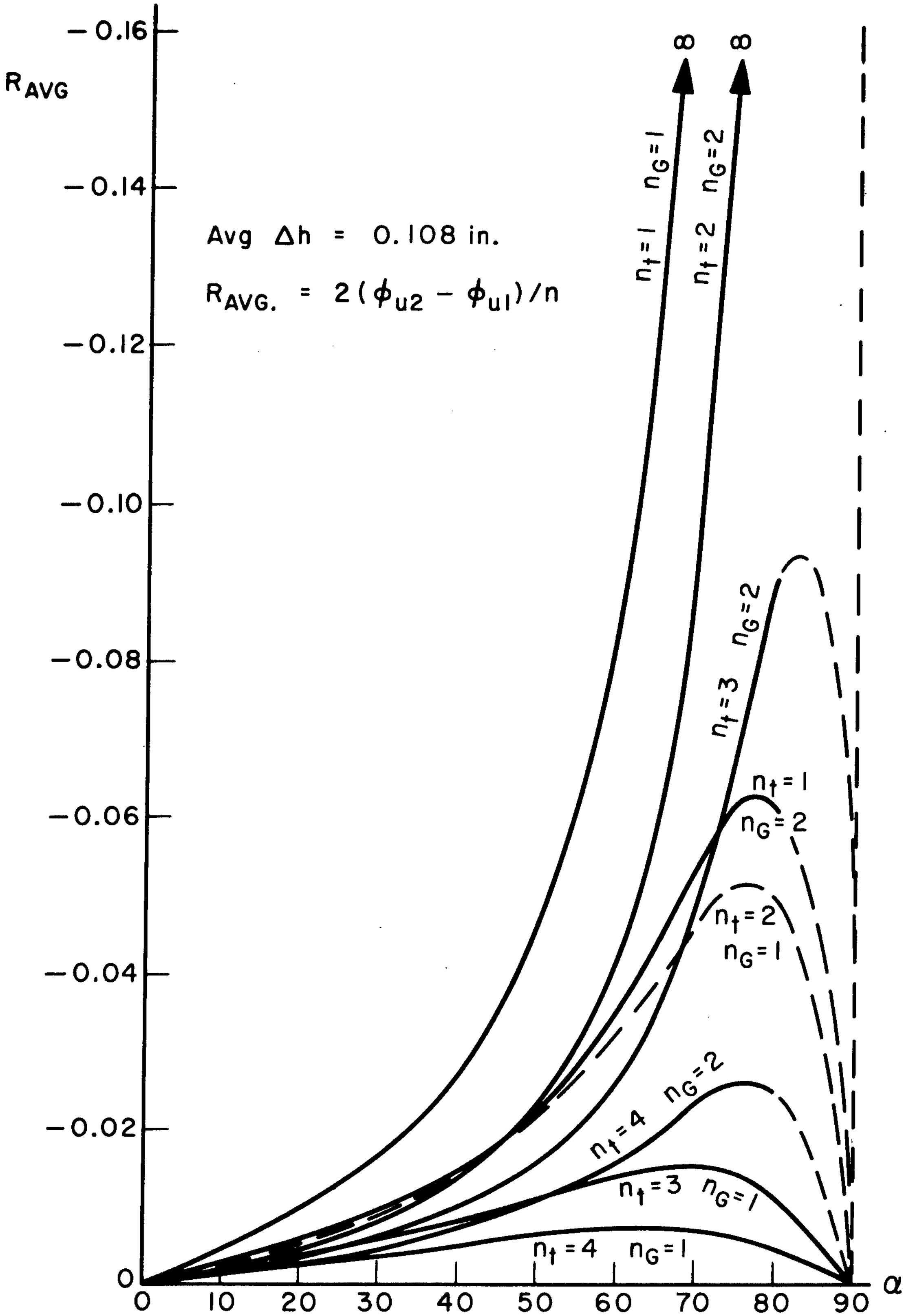

FIG. 3a AVERAGE RATE OF ROTATION (R_{AVG}) IN LOWER COATING vs. THE ANGLE α BETWEEN MEMBRANE AND BENDING OF VARIOUS INTENSITIES. COATING THICKNESS 0.108 in.

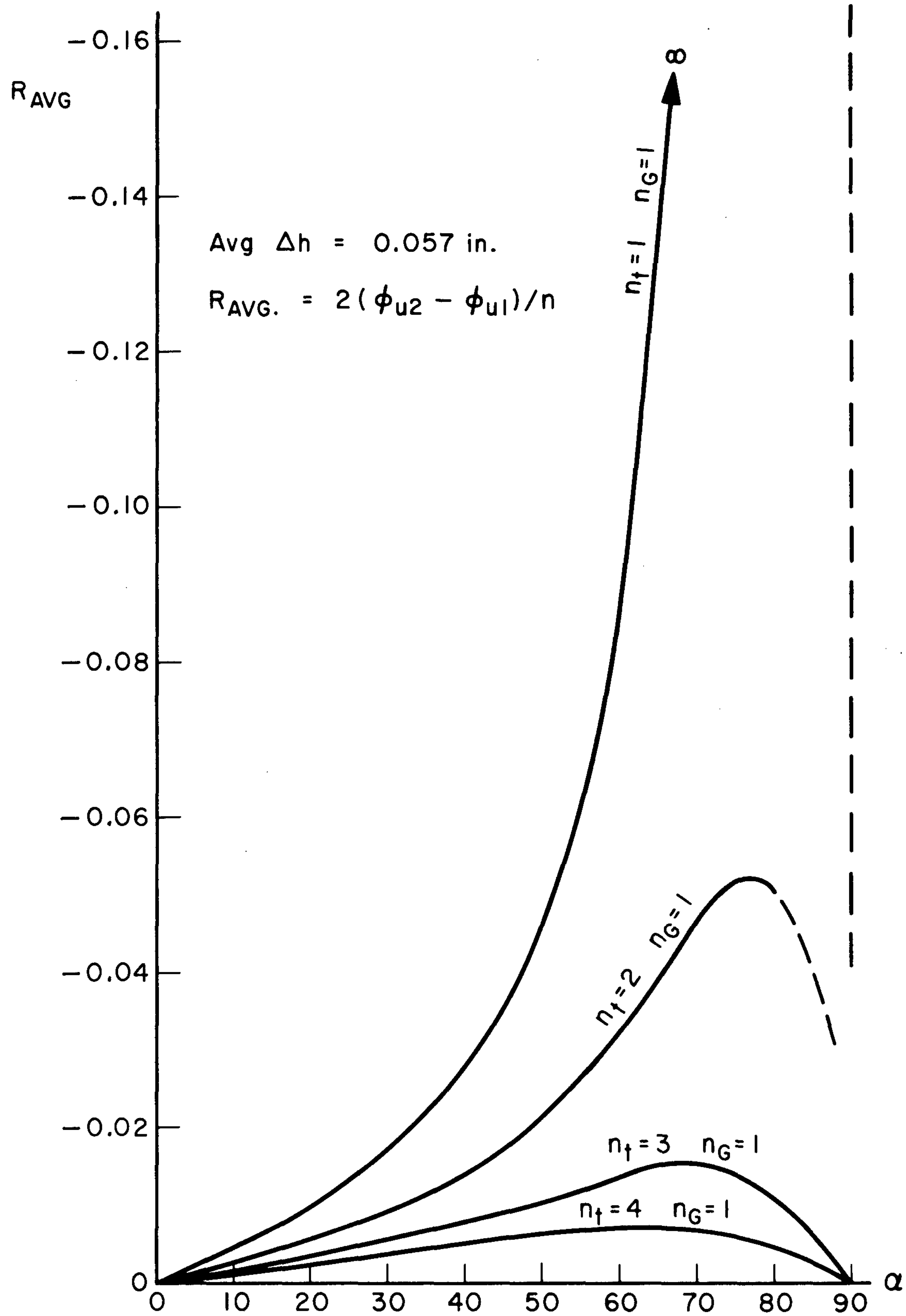

FIG. 3b AVERAGE RATE OF ROTATION (R_{AVG}) IN LOWER COATING vs. THE ANGLE α BETWEEN MEMBRANE AND BENDING OF VARIOUS INTENSITIES. COATING THICKNESS 0.057 in.

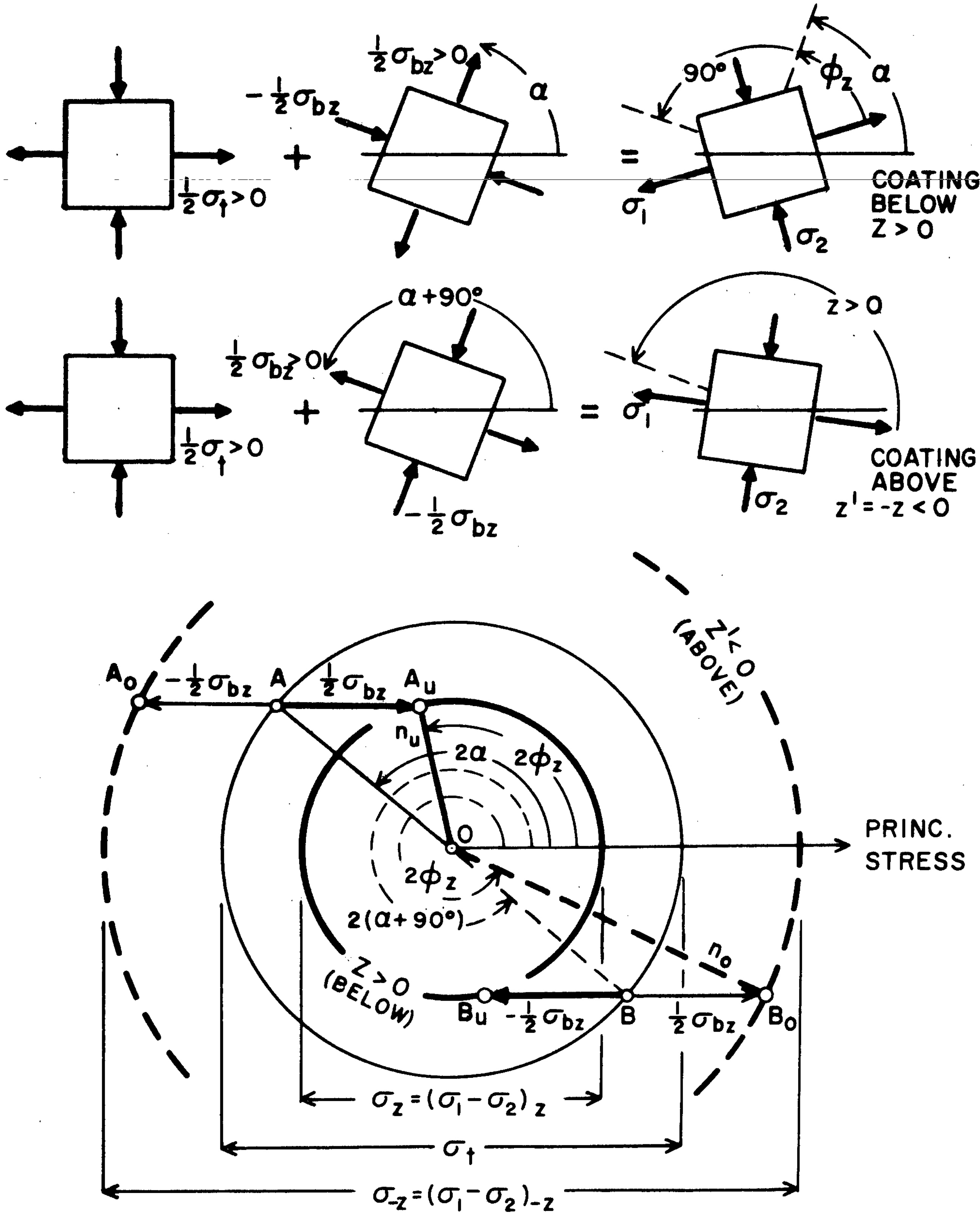

FIG. 4. MOHR DIAGRAM OF THE SUPERPOSITION OF MEMBRANE STRESS σ_t AND BENDING STRESS DIFFERENCE σ_{bz} AT DISTANCE $z > 0$ (COATING BELOW) AND $-z$ (ABOVE). OBSERVATION IS ALWAYS ALONG NORMAL TO SHELL FROM $z > 0$ TOWARD $z < 0$.

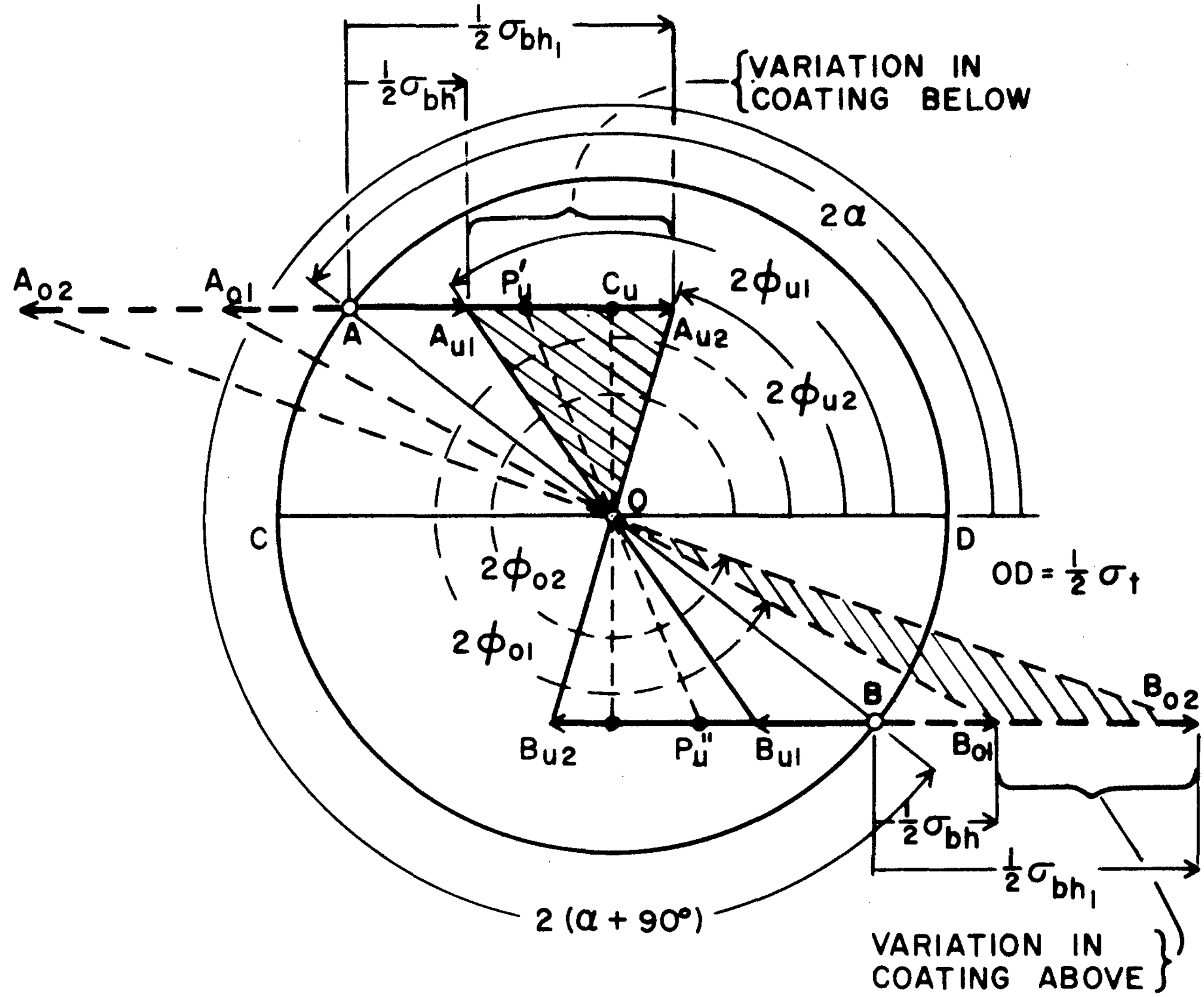

FIG. 5 STRESS VARIATION THROUGH COATING THICKNESS ROTATION $\phi_{u2} - \phi_{u1}$ (BELOW) AND $\phi_{O2} - \phi_{O1}$ (ABOVE). R_{max} OCCURS AT POINT C_u OF LOWER COATING.

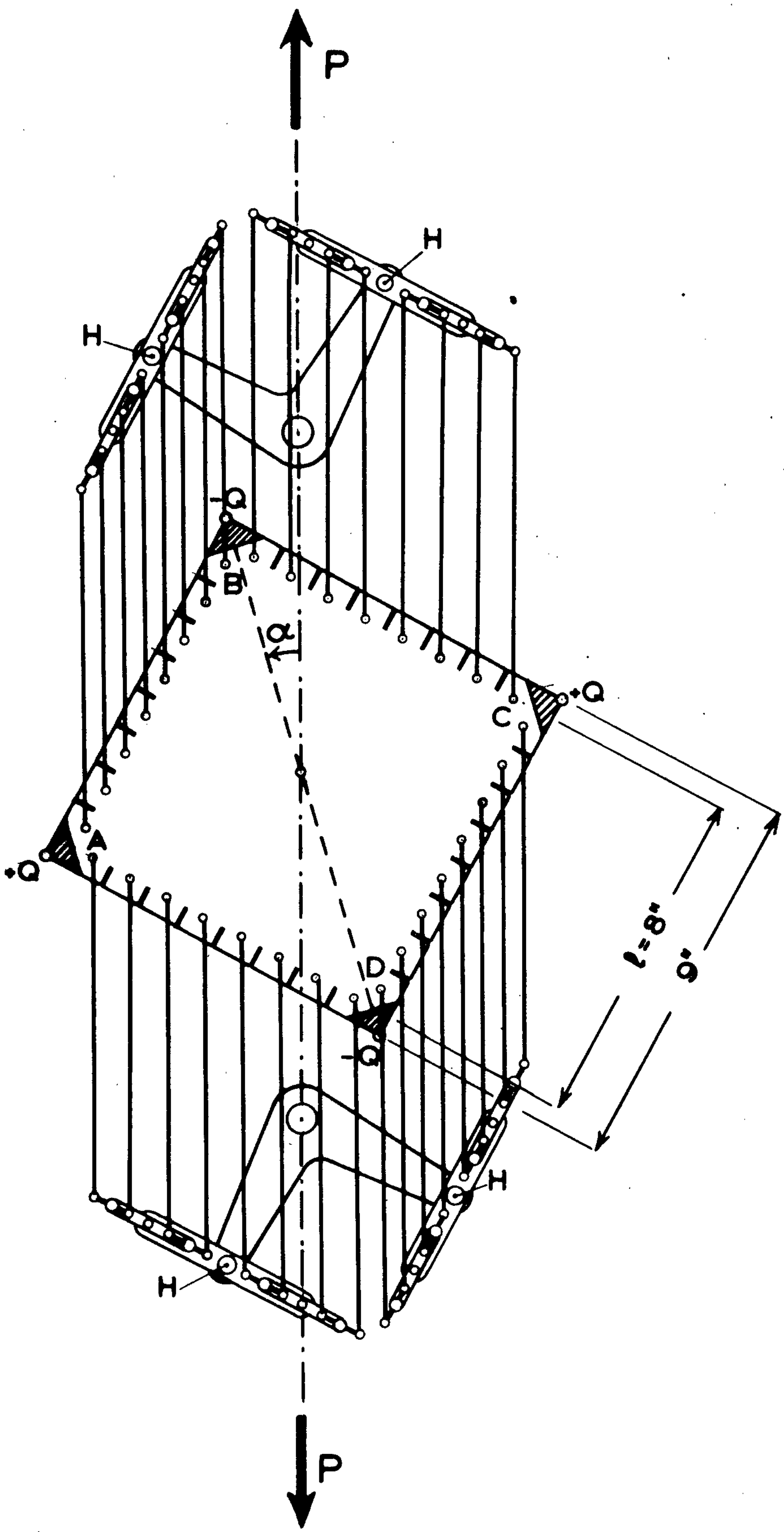

Fig. 6. SCHEMATIC DRAWING OF LOADING SYSTEMS IN SIMPLE TENSION AND ANTICLASTIC BENDING

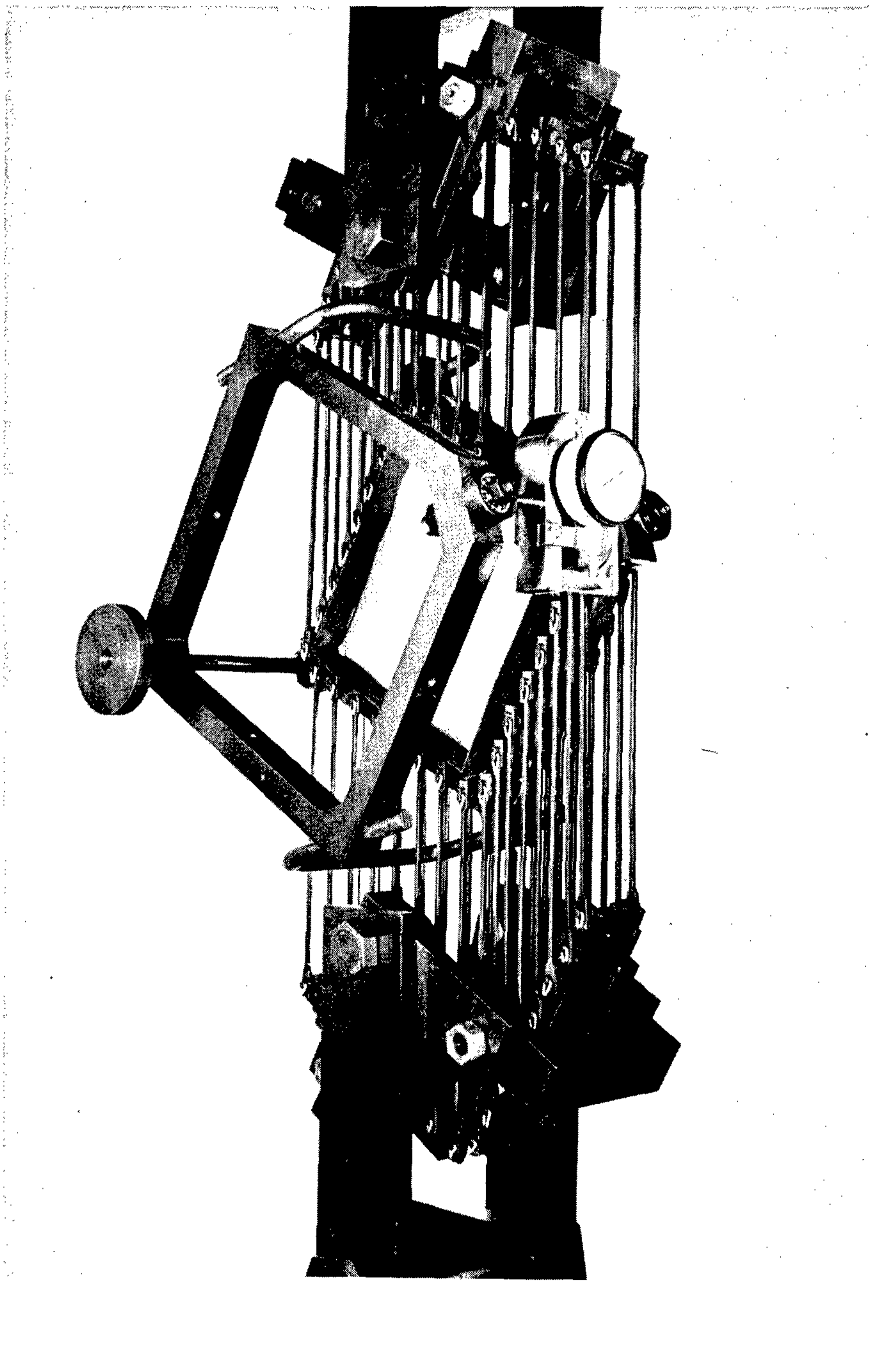

Fig. 7. GENERAL VIEW OF SQUARE PLATE SUBJECTED TO SIMPLE TENSION AND ANTICLASTIC BENDING

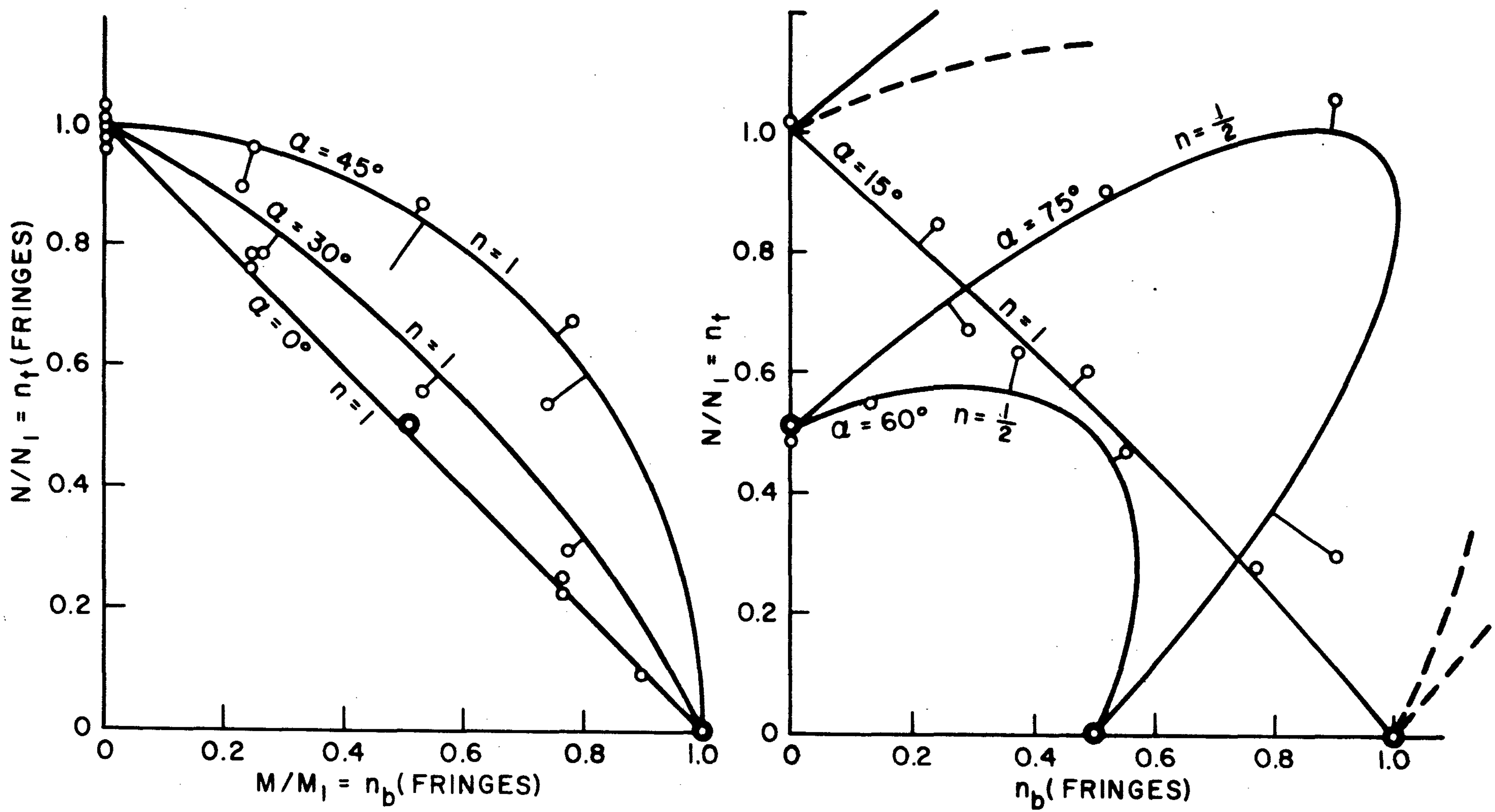

FIG. 8. VALUES OF n_b, n_t PRODUCING ONE FRINGE AT $\alpha = 0°, 15°, 30°, 45°,$ 90° AND ONE-HALF FRINGE AT $\alpha = 60°$ AND 75°.

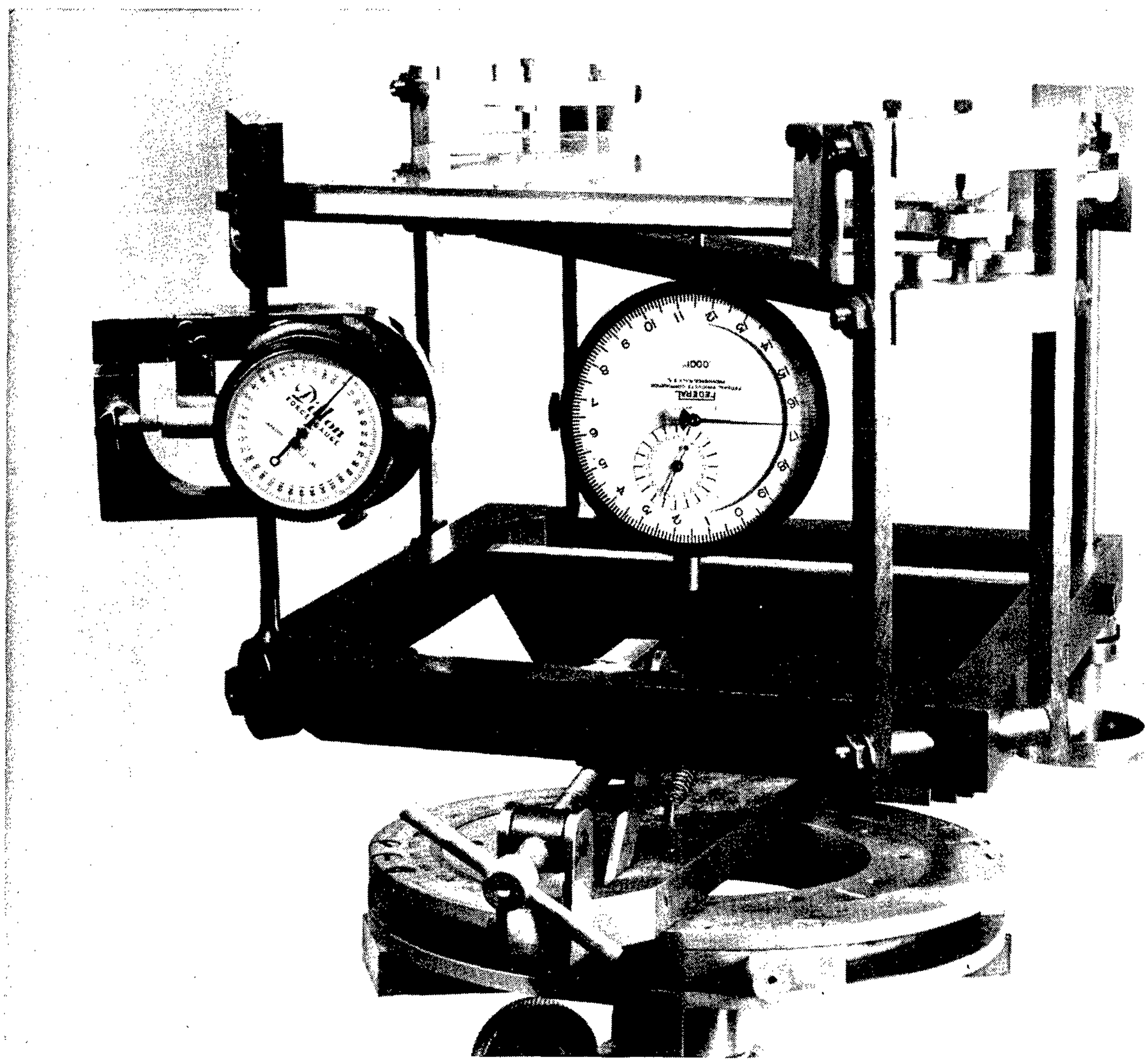

FIG. 9 SQUARE PLATE WITH BIREFRINGENT COATINGS ON BOTH FACES SUBJECTED TO ANTICLASTIC BENDING. DIAL AT LEFT BELONGS TO DYNAMOMETER MEASURING CORNER LOADS. DIAL AT CENTER HANGS FROM DEFLECTOMETER SPANNING FRONT-TO-BACK DIAGONAL. BOTTOM RIGHT KNOB IS FOR LOAD APPLICATION.

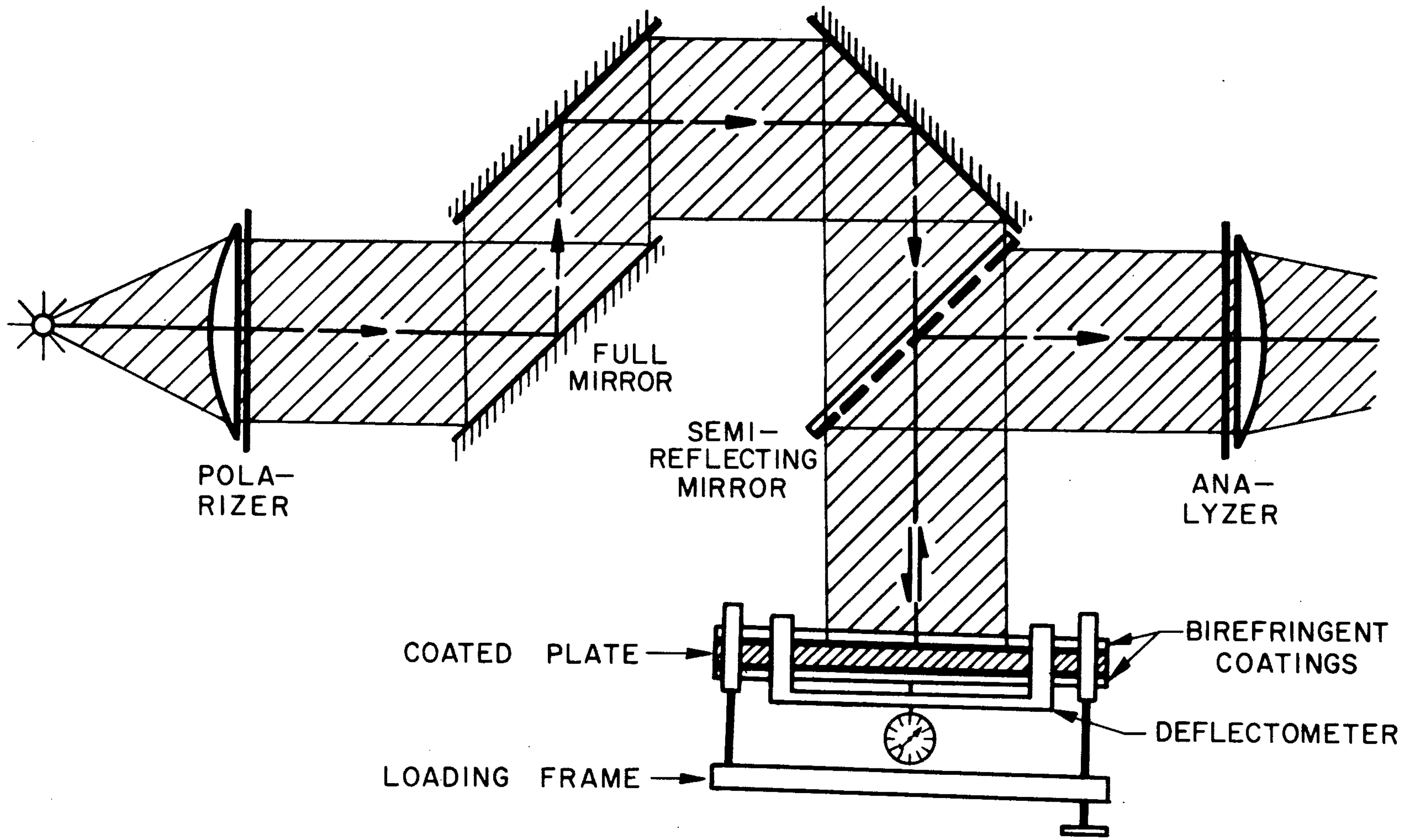

FIG. 10 SCHEMATIC DIAGRAM OF APPARATUS

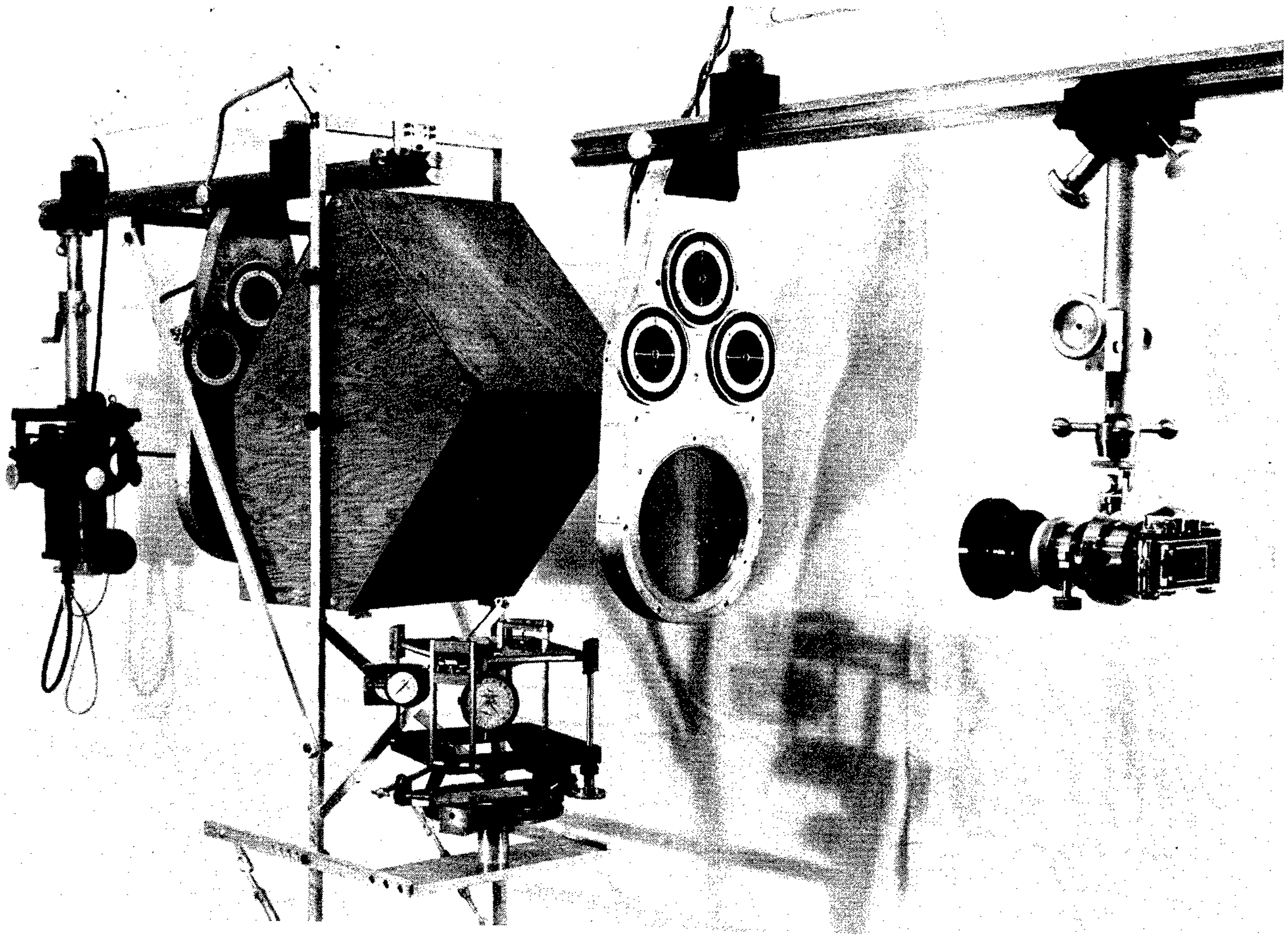

FIG. 11 GENERAL VIEW OF POLARISCOPE AND PLATE IN ANTICLASTIC BENDING OBSERVED AT NORMAL INCIDENCE.

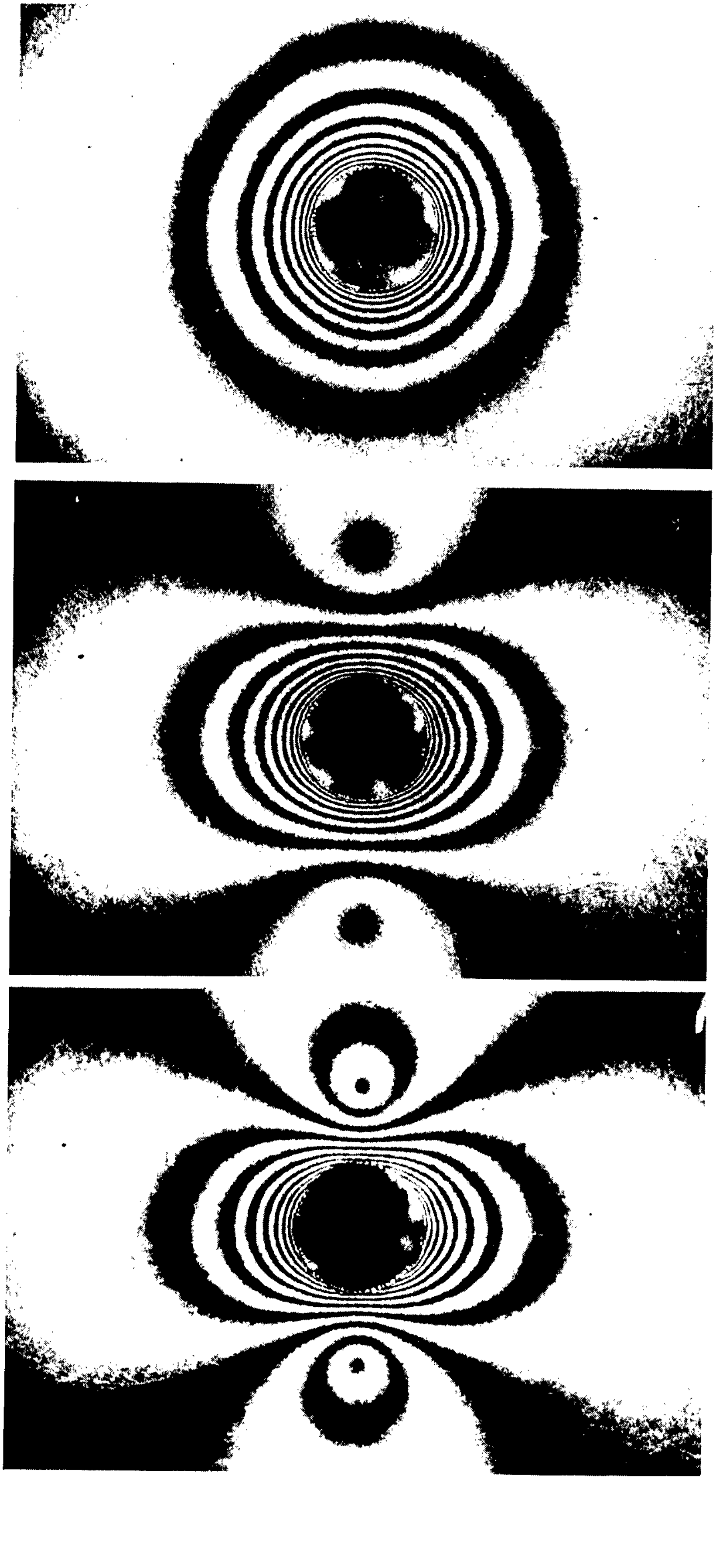

FIG. 12

FRINGE PATTERNS IN LOWER COATING

a. MEMBRANE STRESS ONLY. PRINCIPAL DIRECTIONS ARE CIRCUMFERENTIAL: n_t ; $n_b = 0$

b. BENDING CAUSING ONE FRINGE SUPERIMPOSED ON MEMBRANE STRESS. PRINCIPAL BENDING DIRECTION VERTICAL. n_t ; $n_b = 1$

c. BENDING CAUSING TWO FRINGES SUPERIMPOSED ON MEMBRANE STRESS. PRINCIPAL BENDING DIRECTION VERTICAL. n_t ; $n_b = 2$

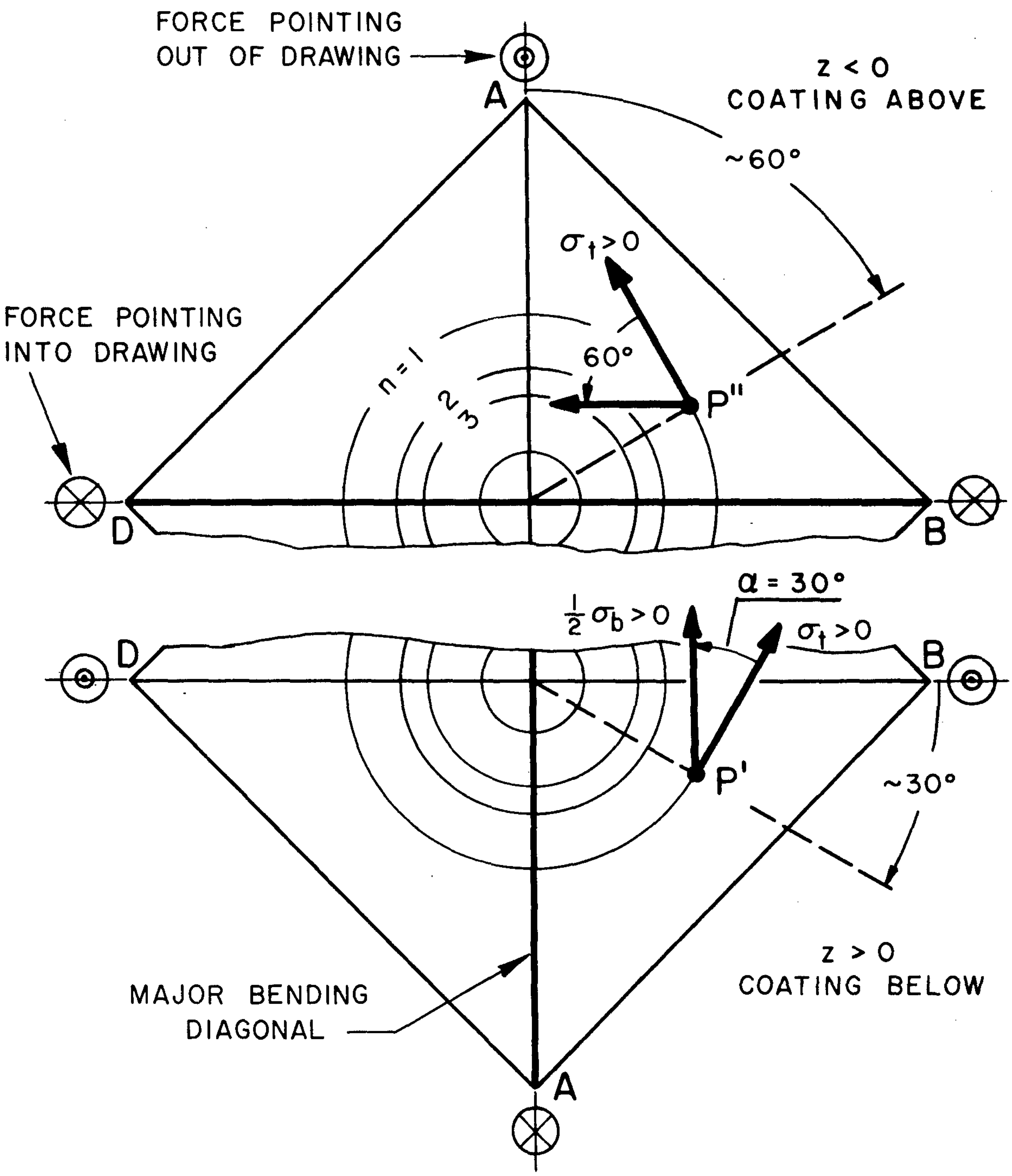

FIG.13. POSITION OF CORRESPONDING POINTS P', P'' IN COATINGS BELOW AND ABOVE AND ANGLES BETWEEN POSITIVE MEMBRANE AND BENDING STRESSES.

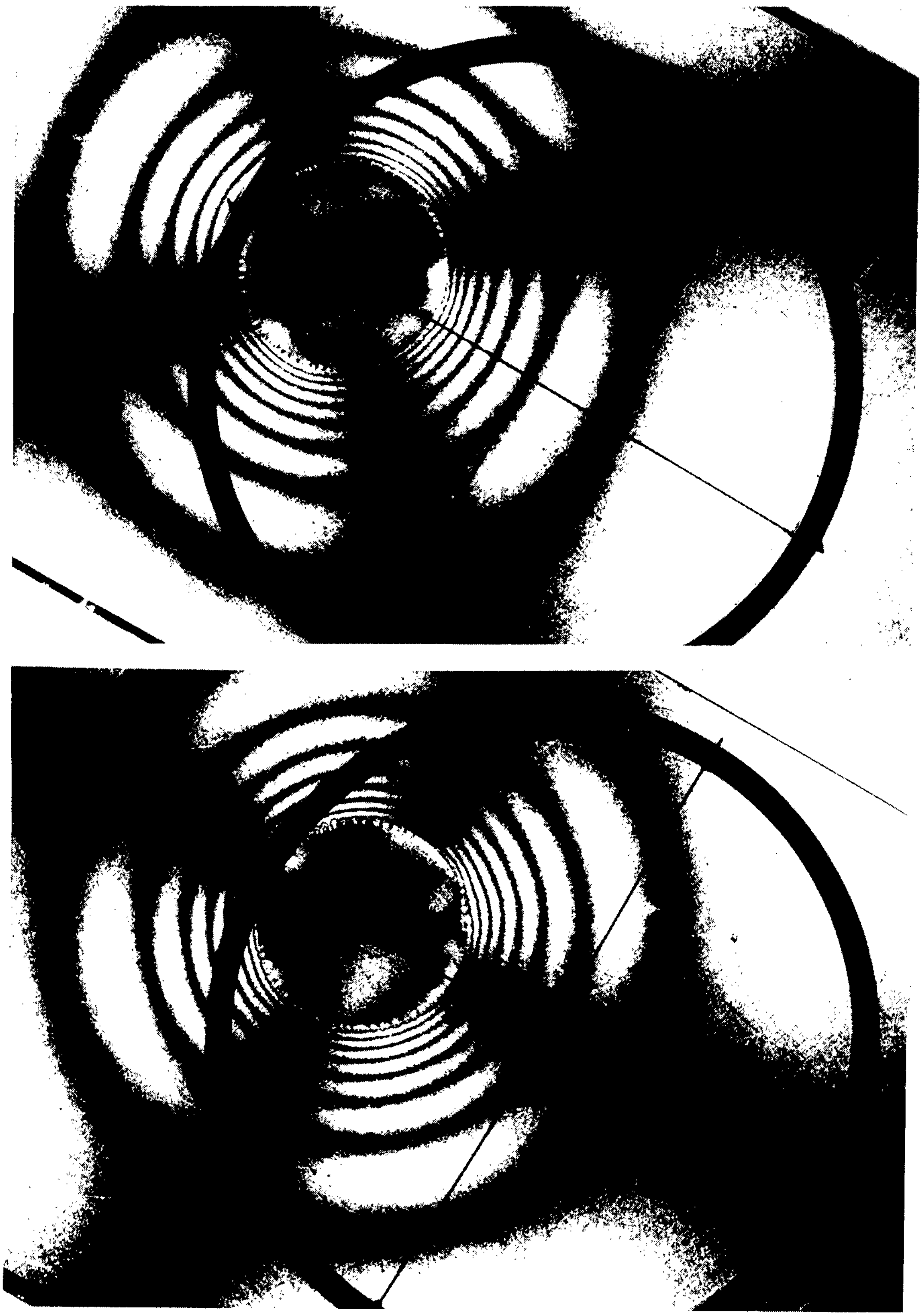

a.

b.

FIG. 14 DETAIL OF PLATE WITH MEMBRANE STRESS ONLY. CROSS - HAIRS AT POINT WITH $n_t = 2$, $n_b = 0$ AND PRINCIPAL DIRECTION AT 30° TO VERTICAL DIAGONAL.
COMPARE WITH FIG. 12 a.

a. PLANE POL. LIGHT AT 45° TO PRINCIPAL STRESS

b. PLANE POL. LIGHT PARALLEL TO PRINCIPAL STRESS

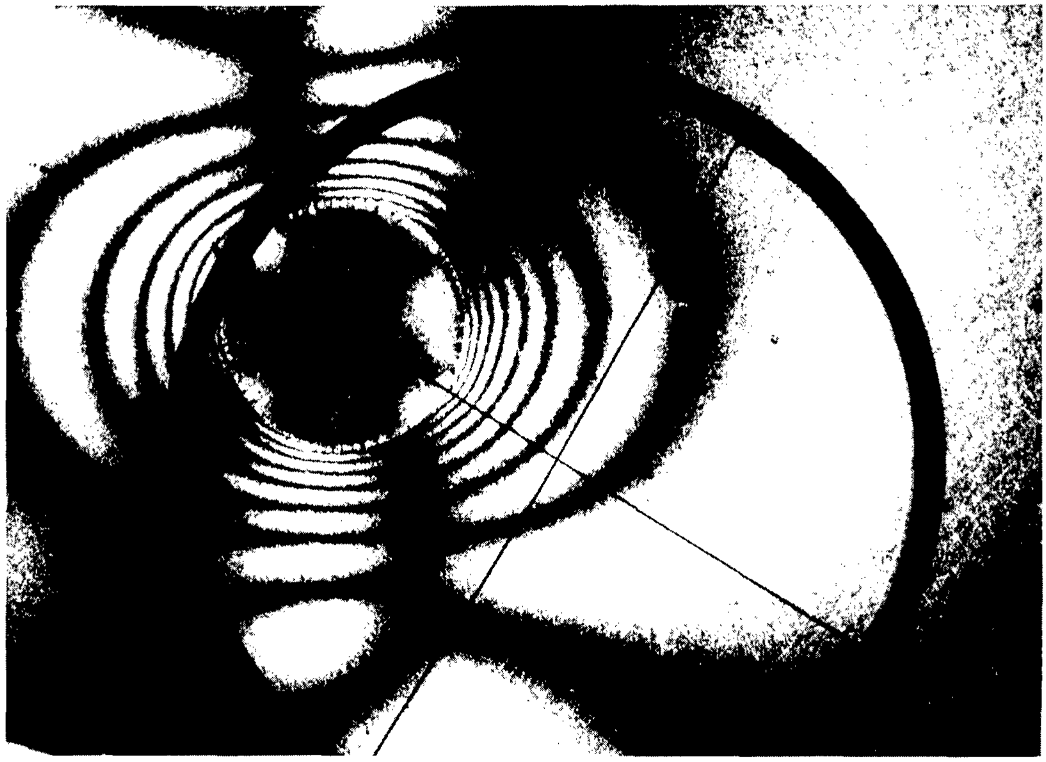

a.

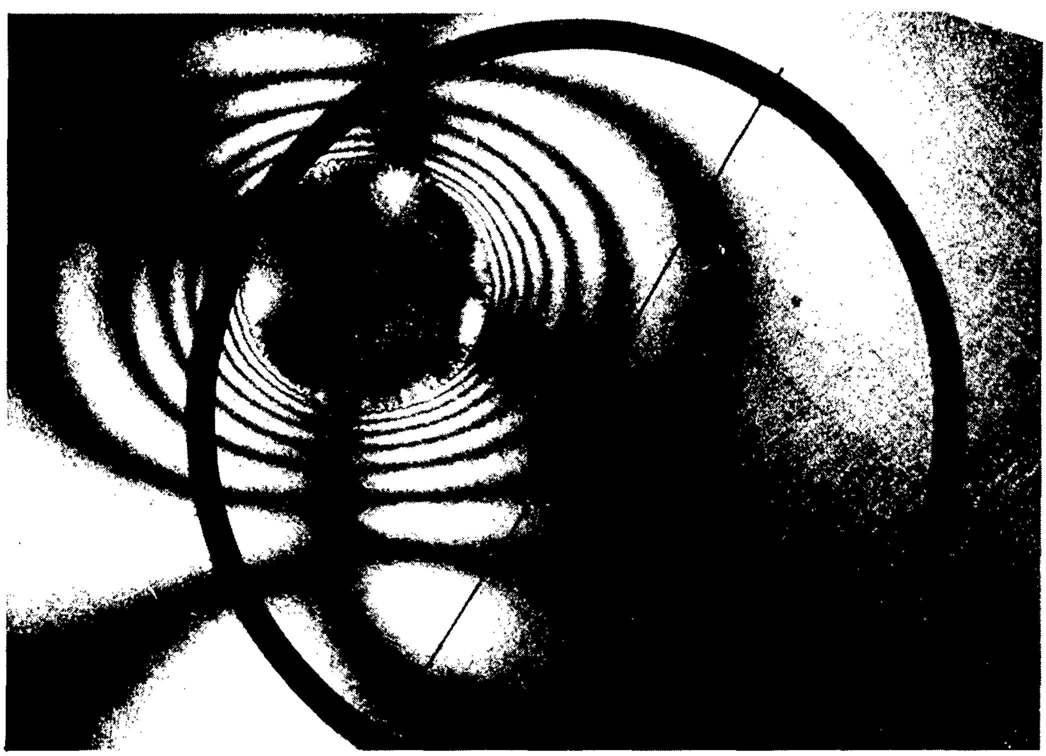

b.

FIG. 15 THE SAME POINT AS IN FIG. 14 WITH A SUPERIMPOSED BENDING CAUSING ONE FRINGE: $n_t = 2$, $n_b = 1$.
COMPARE WITH FIG. 12 b. $n_u = 1.9$.

a. PLANE POL. LIGHT AT 45° TO AZIMUTH OF MINIMUM INTENSITY.

b. PLANE POL. LIGHT AT AZIMUTH OF MINIMUM INTENSITY.

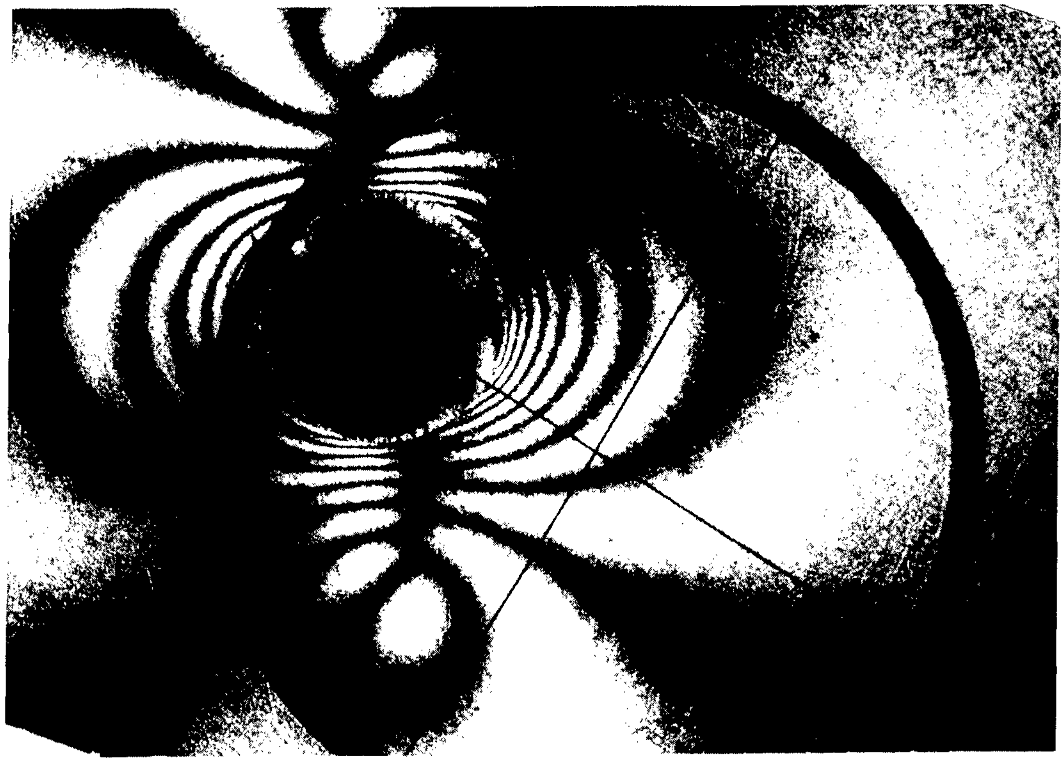

a.

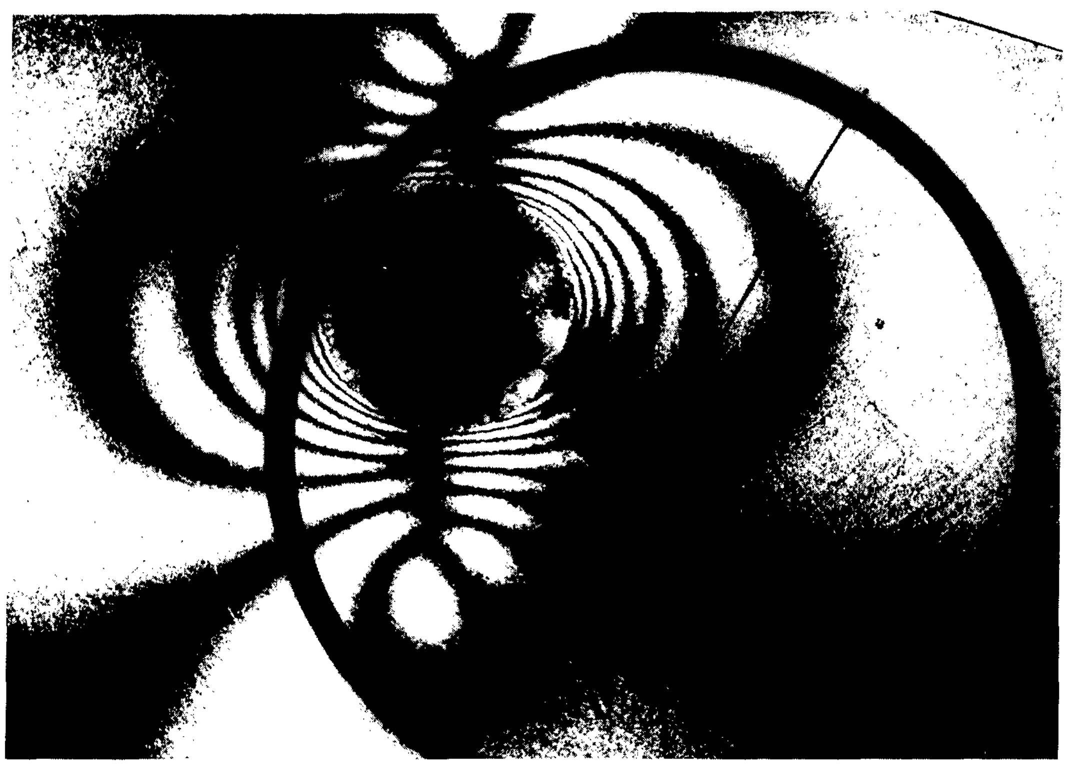

b.

FIG. 16 THE SAME POINT AS IN FIG. 14 WITH A SUPERIMPOSED BENDING CAUSING TWO FRINGES: $n_t = 2$, $n_b = 2$.
COMPARE WITH FIG. 12 b. $n_u = 2.8$.

a. PLANE POL. LIGHT AT 45° TO AZIMUTH OF MINIMUM INTENSITY.
b. PLANE POL. LIGHT AT AZIMUTH OF MINIMUM INTENSITY.

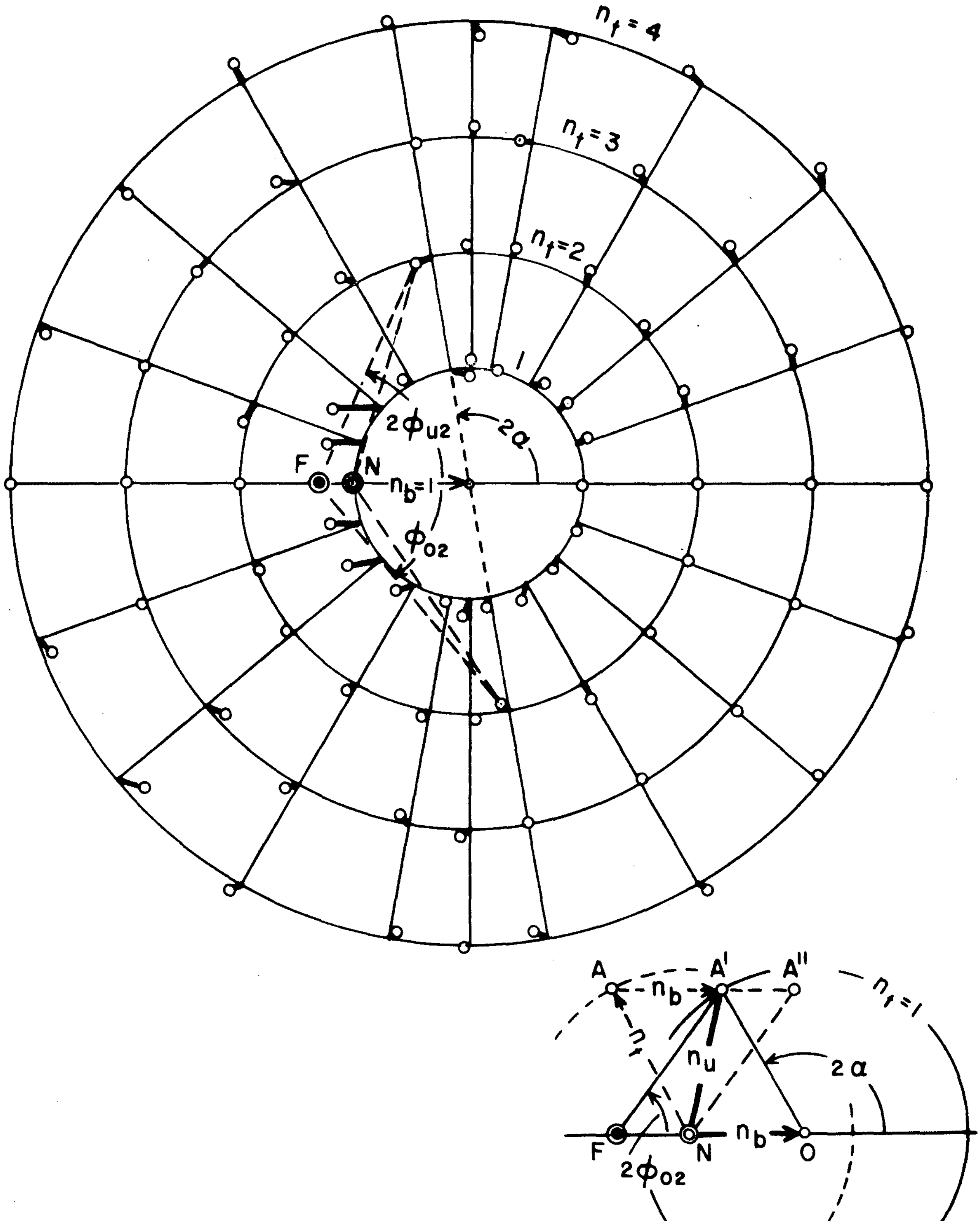

FIG. 17. OBSERVED n_u, ϕ_{u2} AND n_o, ϕ_{o2} PLOTTED ON MOHR'S DIAGRAM FOR COMPARISON WITH THEORETICAL VALUES. COATING THICKNESS $\Delta h = 0.108$ IN. $n_b = 1$; $n_t = 1$ TO 4.

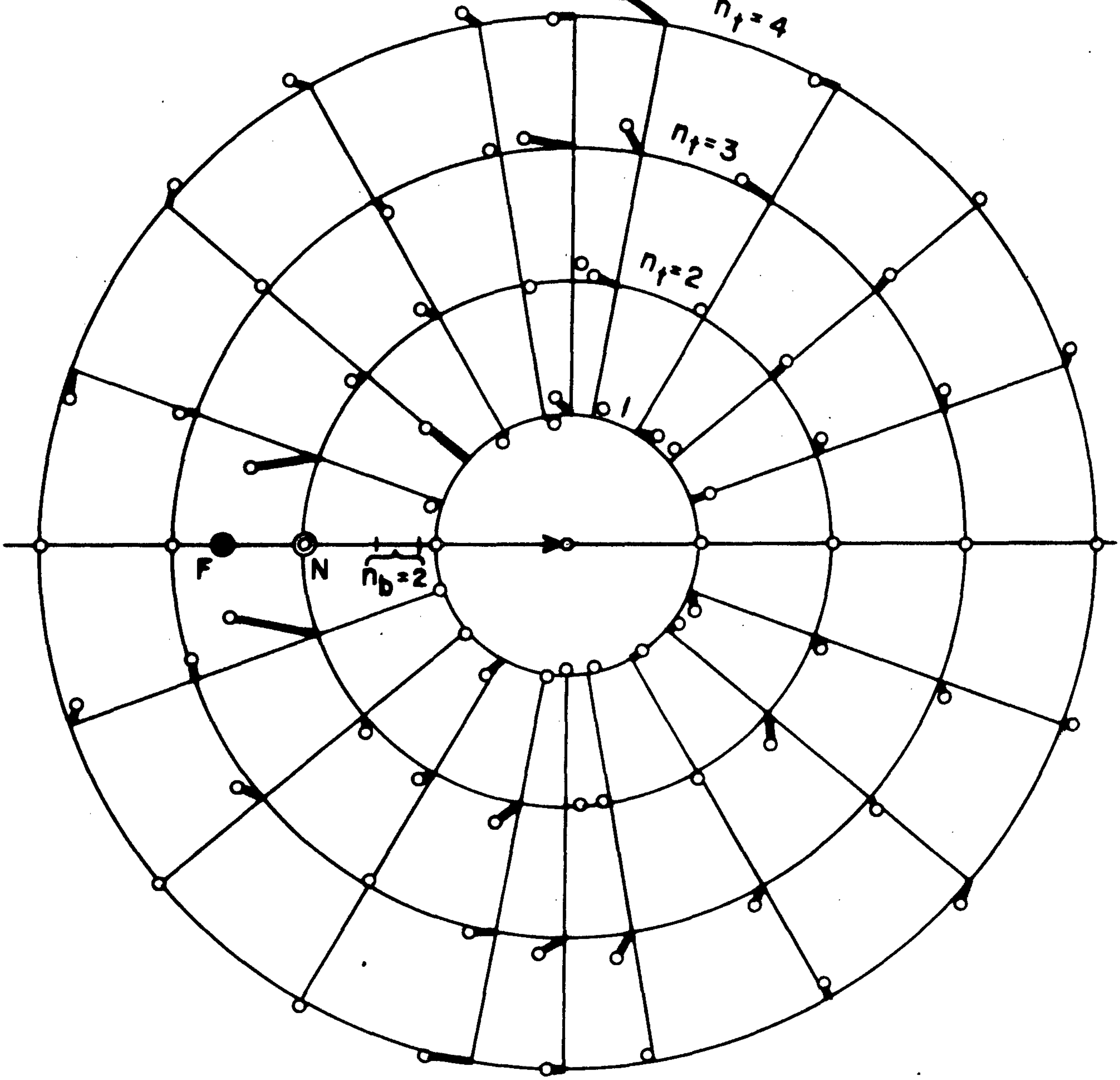

FIG. 18. OBSERVED n_u, ϕ_{u2} AND n_o, ϕ_{o2} PLOTTED ON MOHR'S DIAGRAM FOR COMPARISON WITH THEORETICAL VALUES. COATING THICKNESS $\Delta h = 0.108$ IN. $n_b = 2$; $n_t = 1$ TO 4.

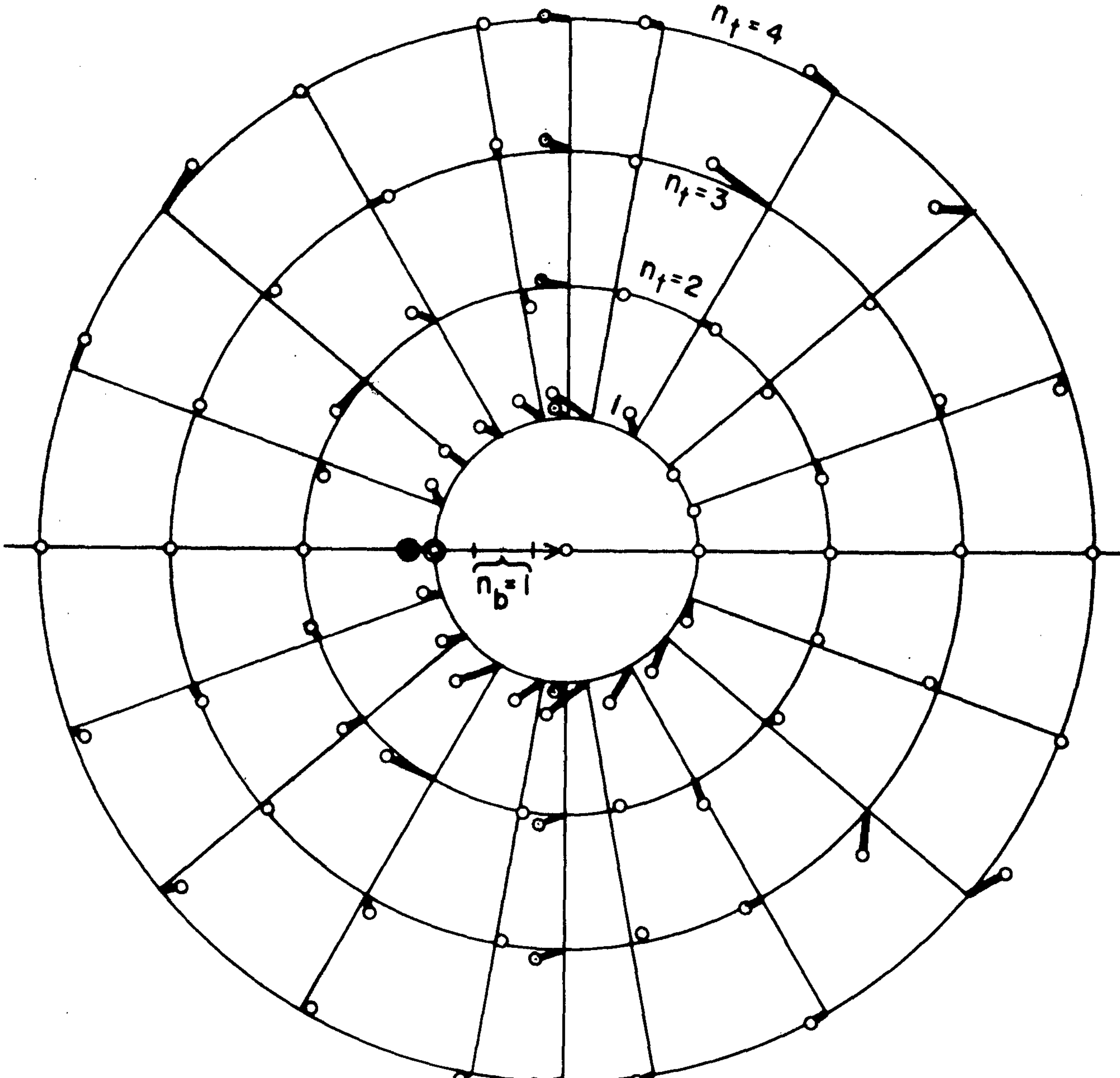

FIG. 19. OBSERVED n_u, ϕ_{u2} AND n_o, ϕ_{o2} PLOTTED ON MOHR'S DIAGRAM FOR COMPARISON WITH THEORETICAL VALUES. COATING THICKNESS $\Delta h = 0.057$ IN. $n_b = 1$; $n_t = 1$ TO 4.

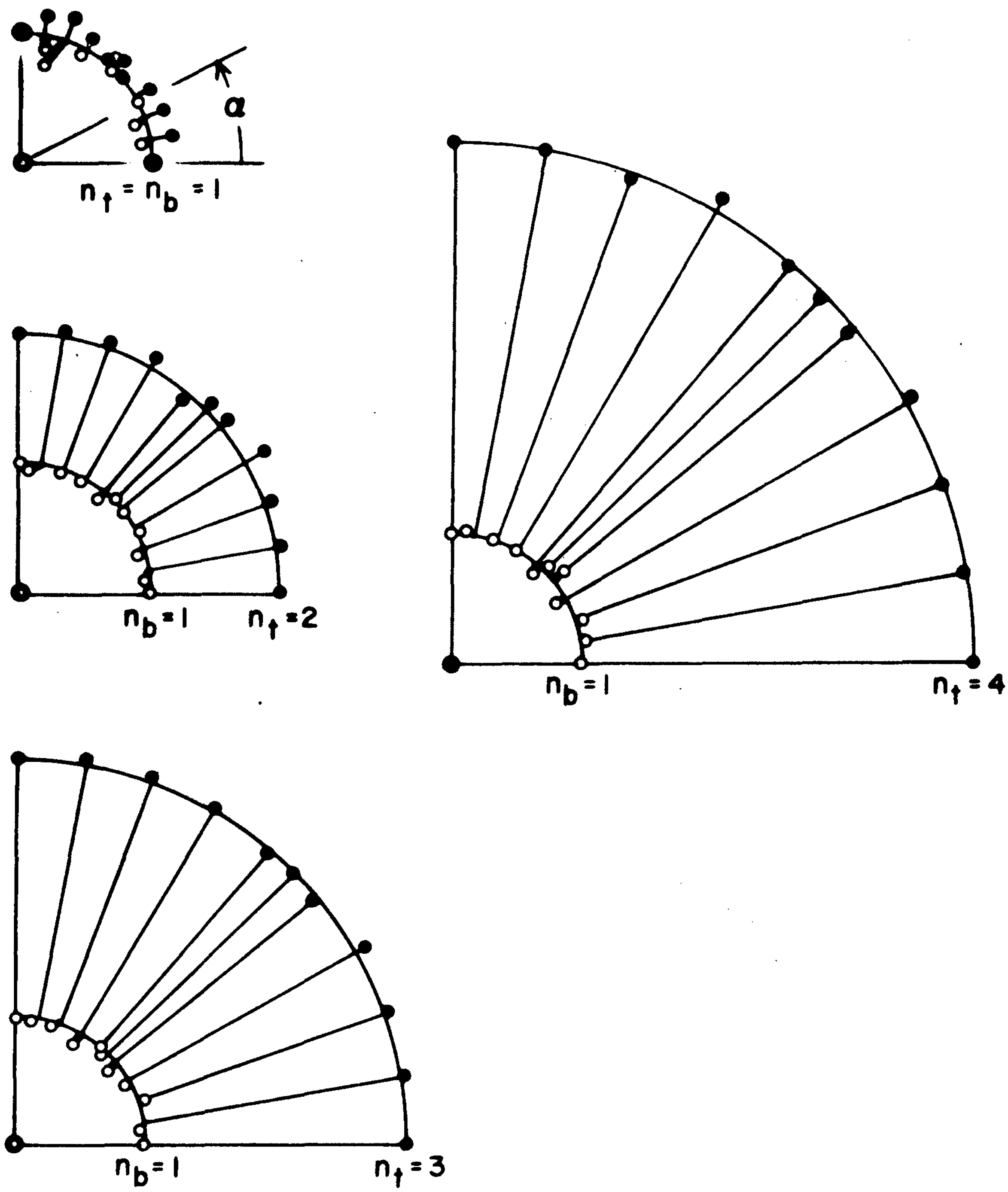

FIG. 20 SOLUTION FOR THE STRESS-DIFFERENCES. EXPERIMENTAL RESULTS SHOWN BY DOTS JOINED TO TRUE VALUE FOR COMPARISON. COATING $\Delta h = 0.108$ IN.; $n_b = 1$.

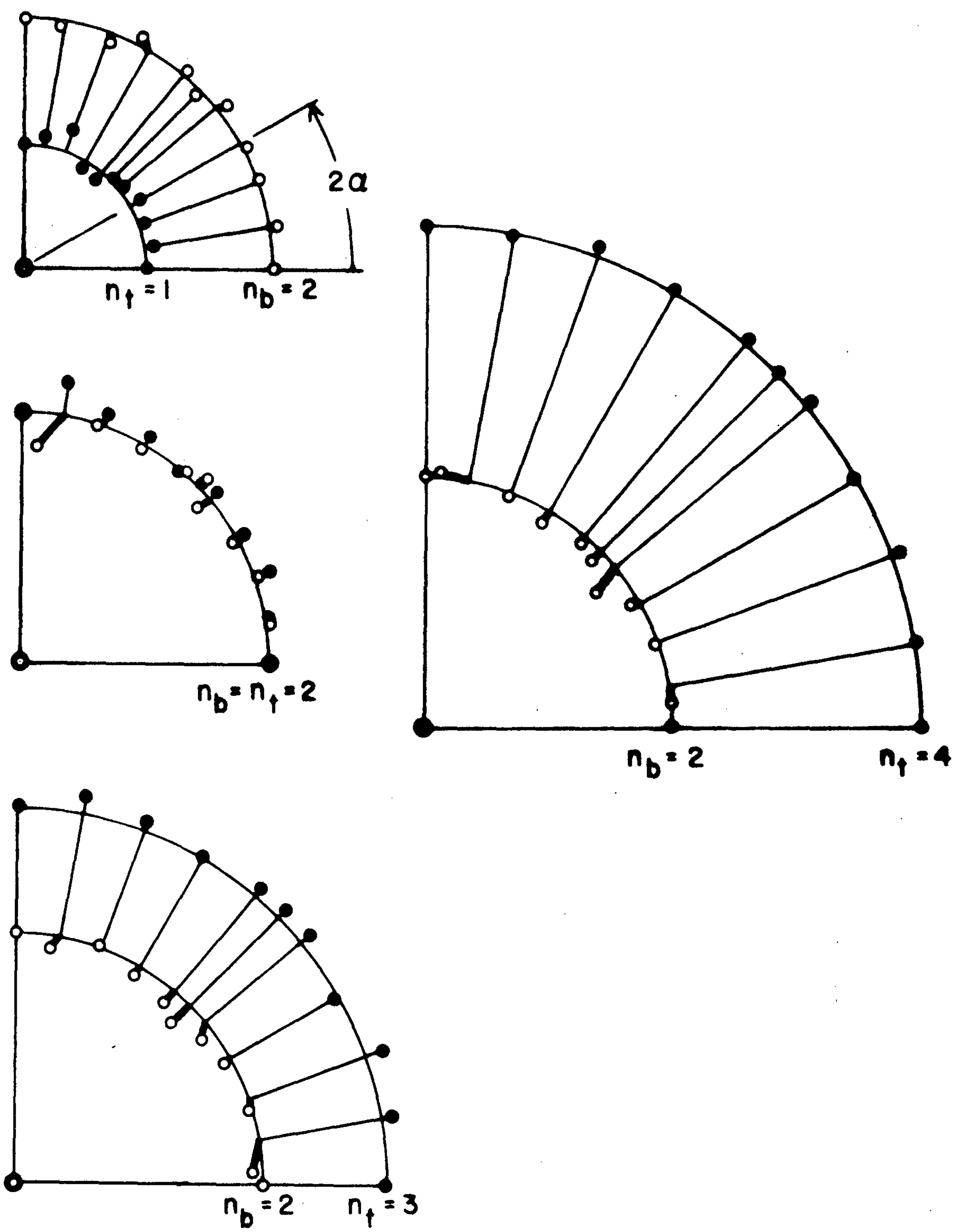

FIG. 21 SOLUTION FOR THE STRESS-DIFFERENCES. EXPERIMENTAL RESULTS SHOWN BY DOTS JOINED TO TRUE VALUE FOR COMPARISON. COATING $\Delta h = 0.108$ in ; $n_b = 2$.

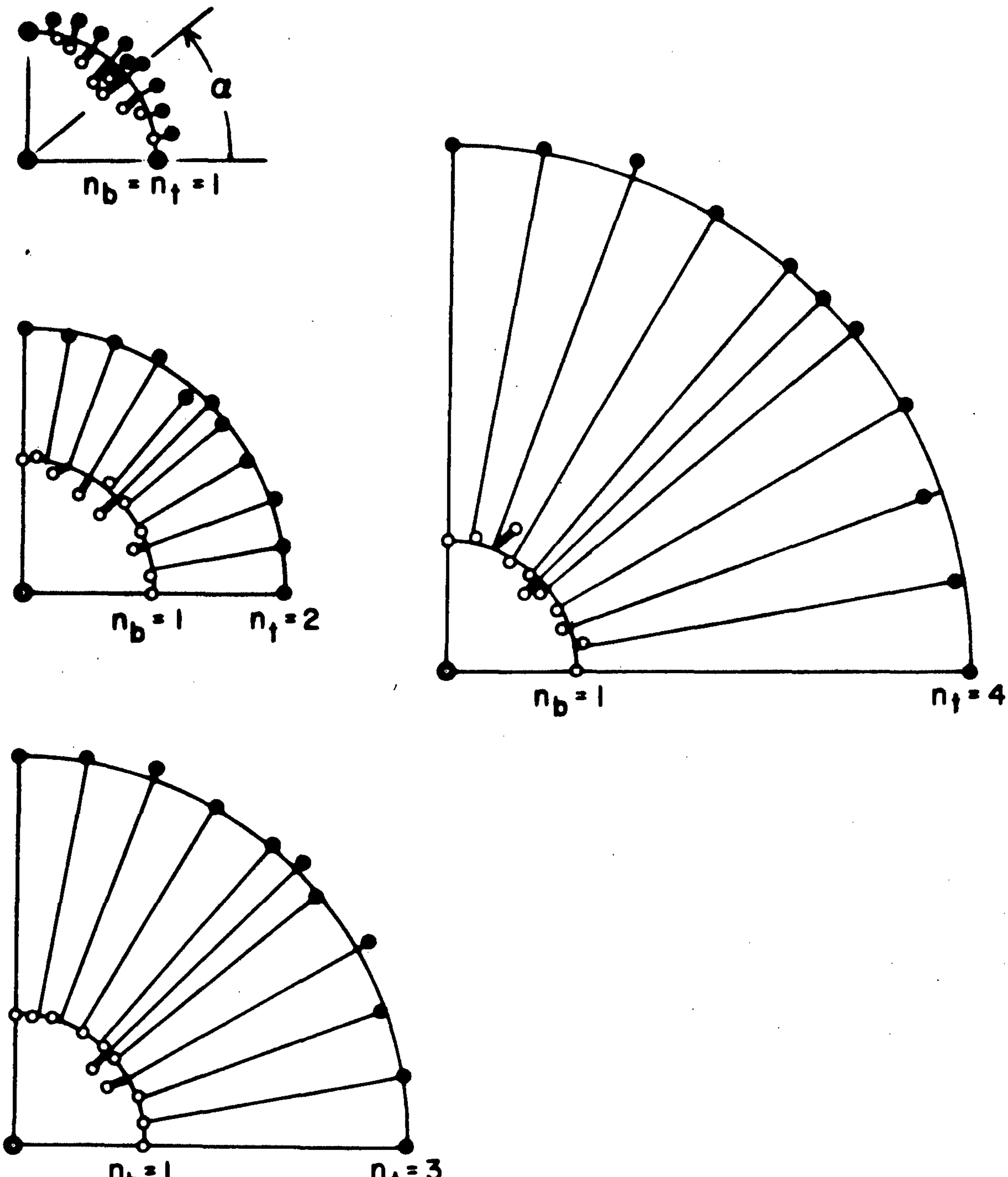

FIG. 22 SOLUTION FOR THE STRESS-DIFFERENCES. EXPERIMENTAL RESULTS SHOWN BY DOTS JOINED TO TRUE VALUE FOR COMPARISON COATING $\Delta h = 0.057$ in; $n_b = 1$.